NAVAL POSTGRADUATE SCHOOL

MONTEREY, CALIFORNIA

THESIS

MULTIRECEIVER ACOUSTIC COMMUNICATIONS IN TIME-VARYING ENVIRONMENTS

by

Murat Aydogmus

June 2014

Thesis Advisor: Roberto Cristi
Second Reader: Joseph Rice

Approved for public release; distribution is unlimited

THIS PAGE INTENTIONALLY LEFT BLANK

REPORT DOCUMENTATION PAGE			*Form Approved OMB No. 0704-0188*
Public reporting burden for this collection of information is estimated to average 1 hour per response, including the time for reviewing instruction, searching existing data sources, gathering and maintaining the data needed, and completing and reviewing the collection of information. Send comments regarding this burden estimate or any other aspect of this collection of information, including suggestions for reducing this burden, to Washington headquarters Services, Directorate for Information Operations and Reports, 1215 Jefferson Davis Highway, Suite 1204, Arlington, VA 22202-4302, and to the Office of Management and Budget, Paperwork Reduction Project (0704-0188) Washington DC 20503.			
1. AGENCY USE ONLY ***(Leave blank)***	**2. REPORT DATE** June 2014	**3. REPORT TYPE AND DATES COVERED** Master's Thesis	
4. TITLE AND SUBTITLE MULTIRECEIVER ACOUSTIC COMMUNICATIONS IN TIME-VARYING ENVIRONMENTS		**5. FUNDING NUMBERS**	
6. AUTHOR(S) Murat Aydogmus			
7. PERFORMING ORGANIZATION NAME(S) AND ADDRESS(ES) Naval Postgraduate School Monterey, CA 93943-5000		**8. PERFORMING ORGANIZATION REPORT NUMBER**	
9. SPONSORING /MONITORING AGENCY NAME(S) AND ADDRESS(ES) N/A		**10. SPONSORING/MONITORING AGENCY REPORT NUMBER**	
11. SUPPLEMENTARY NOTES The views expressed in this thesis are those of the author and do not reflect the official policy or position of the Department of Defense or the U.S. Government. IRB Protocol number ____N/A____.			
12a. DISTRIBUTION / AVAILABILITY STATEMENT Approved for public release; distribution is unlimited		**12b. DISTRIBUTION CODE** A	

13. ABSTRACT (maximum 200 words)

In this thesis, we present a two-receiver underwater acoustic communications system. It is based on the Kalman filter for equalization and tracking of acoustic channels characterized by considerable multipath. To model this channel and its dependency on the ocean environment we use the Bellhop acoustic ray tracing model. Error-correction coding is applied to the source data. Recursively updated channel estimates are used to update the state filters and tracking of the channel. It is shown that, under moderate conditions of Doppler shift and signal-to-noise (SNR) ratio, this algorithm is effective in tracking the channel and reconstructing the transmitted data.

14. SUBJECT TERMS Bellhop, ray-tracing model, Kalman filter, forward-error correction, channel estimation, underwater acoustics, acoustic communications, multipath channel.			**15. NUMBER OF PAGES** 85
			16. PRICE CODE
17. SECURITY CLASSIFICATION OF REPORT Unclassified	**18. SECURITY CLASSIFICATION OF THIS PAGE** Unclassified	**19. SECURITY CLASSIFICATION OF ABSTRACT** Unclassified	**20. LIMITATION OF ABSTRACT** UU

NSN 7540-01-280-5500 Standard Form 298 (Rev. 2-89)
Prescribed by ANSI Std. 239-18

THIS PAGE INTENTIONALLY LEFT BLANK

Approved for public release; distribution is unlimited

MULTIRECEIVER ACOUSTIC COMMUNICATIONS IN TIME-VARYING ENVIRONMENTS

Murat Aydogmus
Lieutenant Junior Grade, Turkish Navy
B.S., Turkish Naval Academy, 2009

Submitted in partial fulfillment of the
requirements for the degrees of

MASTER OF SCIENCE IN ENGINEERING ACOUSTICS

AND

MASTER OF SCIENCE IN ELECTRICAL ENGINEERING

from the

NAVAL POSTGRADUATE SCHOOL
June 2014

Author: Murat Aydogmus

Approved by: Roberto Cristi
Thesis Advisor

Joseph Rice
Second Reader

Daphne Kapolka
Chair, Engineering Acoustics Academic Committee

R. Clark Robertson
Chair, Department of Electrical and Computer Engineering

THIS PAGE INTENTIONALLY LEFT BLANK

ABSTRACT

In this thesis, we present a two-receiver underwater acoustic communications system. It is based on a Kalman filter for equalization and tracking of acoustic channels characterized by considerable multipath. To model this channel and its dependency on the ocean environment we use the Bellhop acoustic ray tracing model. Error-correction coding is applied to the source data. Recursively updated channel estimates are used to update the state filters and tracking of the channel. It is shown that, under moderate conditions of Doppler shift and signal-to-noise (SNR) ratio, this algorithm is effective in tracking the channel and reconstructing the transmitted data.

THIS PAGE INTENTIONALLY LEFT BLANK

TABLE OF CONTENTS

LIST OF FIGURES

LIST OF ACRONYMS AND ABBREVIATIONS

ASK	Amplitude-Shift Keying
AWGN	Additive White Gaussian Noise
BER	Bit-Error-Rate
BFSK	Binary Frequency-Shift Keying
BPSK	Binary Phase-Shift Keying
CC	Convolutional Coding
DFE	Decision-Feedback Equalization
DSSS	Direct-Sequence Spread Spectrum
ECC	Error-Correction Coding
FEC	Forward Error Correction
FFT	Fast Fourier Transform
HR-DSSS	High-Reliable DSSS
ISI	Inter-Symbol Interference
K-LMS	Kalman Equalization with LMS
K-RLS	Kalman Equalization with RLS
LMS	Least Mean Squares
MIMO	Multiple-Input Multiple-Output
MMSE	Minimum Mean-Square Error
OFDM	Orthogonal Frequency-Division Multiplexing
OSI	Open Systems Interconnection
PSD	Power Spectral Density
PSK	Phase-Shift Keying
QAM	Quadrature Amplitude Modulation
QPSK	Quadrature Phase-Shift Keying
RLS	Recursive Least Squares
SIMO	Single-Input Multi-Output
SNR	Signal-to-Noise Ratio
TL	Transmission Loss

THIS PAGE INTENTIONALLY LEFT BLANK

EXECUTIVE SUMMARY

The purpose of this thesis is to design a robust underwater communications system that addresses the constraints of the environment and is suitable to a changing environment. It is well known that the underwater medium is particularly challenging to wireless communications, more than the air medium itself. This is due to the slower speed of propagation and the sensitivity to environmental conditions such as boundaries which result in multipath reflections, changing sound speed due to temperature, salinity, and pressure gradients in the water column, wave actions and bottom characteristics.

In this thesis, a combination of optimal filtering, channel estimation and error correction coding are the basis of the proposed approach.

In particular, the main approach presented is based on the application of the Kalman filter to the processing of a two-receiver underwater acoustic communications system. The Kalman filter provides for equalization and tracking of the acoustic channels characterized by considerable multipath due to reflections and varying sound speed. A multiple-receiver approach provides an estimation of the transmitted sequence by interpreting the transmitted data as the state of the dynamic system.

In conjunction with a Kalman filter, error-correction coding (ECC) provides a reliable sequence for channel tracking. In particular, the ECC approach is used to cope with the noise and the distortion problem in the communications environment. Forward error correction (FEC) is used in the simulation, and the convolutional code rate of $1/2$ is applied. The modulation scheme proposed for this thesis is the standard single carrier quadrature phase-shift keying (QPSK).

In order to model the acoustic channel, an artificial channel is created using the Bellhop ray tracing model. The dependencies of the ocean environment are computed and depicted with graphs by this model. Data taken from the Bellhop model are used to capture the Rayleigh fading nature of the underwater channel, which is a representative model for underwater communications. Two different channel receptions are used to estimate the transmitted data sequence, and the channel impulse response coefficients are

predicted by using the least mean squares (LMS) algorithm. Based on the expected Doppler-shift, the estimated channel coefficients are used to recursively generate the Kalman state filters for different values of the signal-to-noise ratio (SNR).

In order to verify the effectiveness of the proposed system, the performance of the Kalman estimator is first tested on static channels and is then evaluated for time-varying channels. Performance of the system is measured by calculating the mean squares error measurements of the channel estimations, and the estimation errors are depicted on a graph for different values of Doppler shift and SNR.

ACKNOWLEDGMENTS

I would like to thank my advisor Professor Roberto Cristi for his great explanations, guidance, and patience. I always received constant support from him, which gave me self-confidence.

I wish to thank Professor Joseph Rice for his support and motivation in his retirement days.

To Paul Baxley, for giving me support while learning the Bellhop model and spending his valuable time with me.

To my beloved wife, Filiz, for always believing in me and supporting me during this thesis research.

To my family, for always showing their smiling faces and credit to me.

Finally, I would like to express my gratitude to the Turkish Navy for giving me the great opportunity to acquire a degree from a great school.

THIS PAGE INTENTIONALLY LEFT BLANK

I. INTRODUCTION

A. THESIS OBJECTIVES

Underwater acoustic communication has a very important role in many applications. In this environment, information is carried by sound waves which propagate in the ocean. This cannot be done effectively by electromagnetic waves, since they are strongly attenuated by water.

The medium for underwater communications is particularly challenging due to a number of factors such as the speed of propagation varying with the water depth. In most channel geometries, there exists multipath propagation, so that the transmitted waveform reaches the receiver through different channels at different times. In addition, acoustic noise generated by marine life and vessel traffic is a factor in the design of a reliable communications system. In numerous studies, a number of underwater communications systems have been investigated, and some approaches have been developed in order to overcome the channel impairments in the underwater environment. One of the important issues to be addressed is channel equalization, which lessens the impact of multipath on inter-symbol interference (ISI).

Previous work by Desselarmos [1] has yielded an estimator that handles the variations in the channel adaptively, and a Kalman filter approach was used to estimate the transmitted sequence and update the state filters adaptively. The demodulation of a signal, assuming the channel is initially estimated using a training sequence and then tracked with an adaptive algorithm, is investigated in this thesis. The demodulation itself is carried out by combining the reception of two receivers using a Kalman filter. In this thesis, the acoustic channel parameters are simulated using the Bellhop ray tracing model. The impulse response produced by the model is used to represent the time-varying channel as a Rayleigh fading channel.

The objective of this thesis is to investigate a communications system in a time-varying underwater acoustic channel by using error correction coding, single carrier modulation and a Kalman filter to estimate past channel values and track variations.

A two-receiver underwater acoustic communications system is proposed, and its performance in tracking channel variations is investigated.

B. THESIS ORGANIZATION

The thesis is organized into seven chapters including the introduction. Underwater networks as the motivation for this work are introduced, and some important developments in the recent years in underwater communications are described in Chapter II. Some fundamental definitions of the underwater environment and some challenges related to underwater communications are discussed in Chapter III. In Chapter IV, the description of the Bellhop ray tracing model, the input file to run the program, and some of the output files used in this thesis are presented. Theoretical development and the experimental setup of the communications system are explored in Chapter V, and results are presented in Chapter VI. Finally, the conclusion of the research and recommendations for future work are discussed in Chapter VII.

II. MOTIVATION AND BACKGROUND

A. UNDERWATER NETWORKS

Underwater communications systems are gaining importance in both civilian and military applications. It is well known that the underwater channel is particularly challenging, and its characteristics differ considerably from the air medium. Since seawater attenuates electromagnetic waves preventing their propagation in underwater environments, the information is sent using acoustic waves. A good understanding and physics-based modeling of the underwater environment is very important for the design and implementation of a reliable underwater communications system. The differences in electromagnetic and acoustic channels require differences in networking protocols in underwater environments compared to radio networks [2].

Sound wave propagation in the ocean is characterized by multipath, Doppler spread, and shadow zones. Due to these channel impairments, underwater communications require an appropriate modulation scheme to have robust communications [3].

One of the major differences for underwater communications with respect to that of the air medium is the propagation velocity. Information sent through radio channels in the air medium propagates at the speed of light, which is relatively constant. On the other hand, the propagation velocity of the acoustic waves through the underwater channel is strongly influenced by environmental conditions such as temperature, salinity, and pressure. The fact that velocity of propagation is on the order of ~1500 m/s, and transmission frequencies are on the order of 10 KHz, implies that Doppler shifts resulting from motion of currents, surface waves, and transmitter and/or receiver have to be taken into account [4].

Radio networking protocols require certain adaptations for effectiveness in the underwater acoustic channel. For underwater environments, most aspects of the protocol have to be reconsidered, including modulation of the transmitted signal, packet

formatting, error correction coding (ECC), error detection methods, medium access control, addressing, and routing.

Under these considerations, a number of methods have been proposed for underwater communications protocols. The Open Systems Interconnection (OSI) model has been followed in the design of underwater networks [2]. For a few decades, various communications and network schemes have been proposed and implemented with some measure of success. In Figure 1, a representative network of underwater nodes is illustrated.

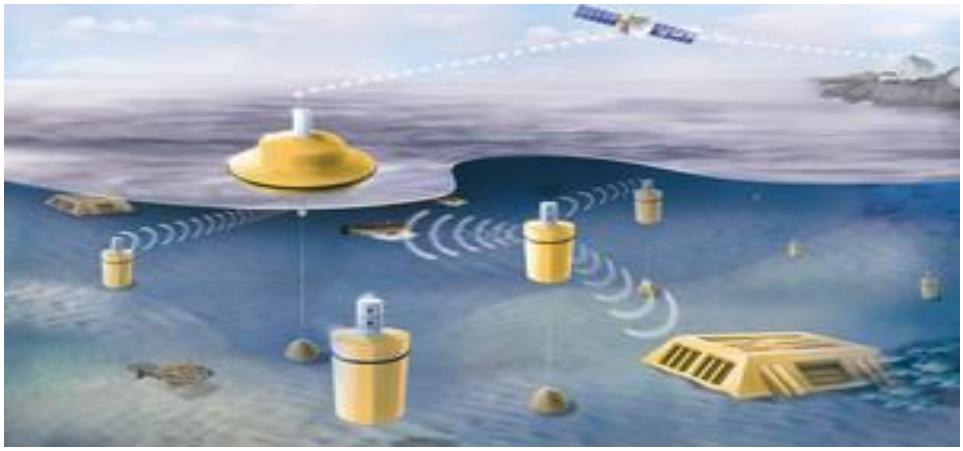

Figure 1. Underwater nodes (from [5]).

B. CHALLENGES OF UNDERWATER ACOUSTIC COMMUNICATIONS

In order to design a robust underwater acoustic communication link, the features of the underwater channel and physical impairments that constrain the channel must be well understood.

The most important constraints that must be taken into account include [1]:

- Propagation latency is much greater than in radio frequency channels because of the relatively slow speed of sound through water.
- The acoustic bandwidth is limited under water, so the communications bandwidth is correspondingly limited.
- There are a number of ambient noise sources which behave generally in a non-Gaussian manner.

- Water currents and tidal currents create instability in the position of nodes, which can make the topology dynamic.
- Multipath propagation causes time-spreading of the received signal with implications for fading and ISI.
- Motion of the transmitter and the receiver causes a Doppler shift effect which must be taken into account.
- The battery-powered underwater nodes cannot be recharged easily like their counterparts in terrestrial networks. Except for nodes at the sea surface, solar energy is not available [1], [6], [7].

Multipath propagation and the Doppler shift are fundamentally important for underwater communications quality compared to other constraints and robust systems have to be designed to handle these impairments.

C. APPROACHES TO UNDERWATER ACOUSTIC COMMUNICATIONS

There have been important developments for underwater acoustic communications systems in order to achieve higher data rates. Some of these developments are explained below.

1. Multiple-Input Multiple-Output (MIMO)

A Multiple-Input Multiple-Output (MIMO) system is a structure involving multiple transmitters and multiple receivers in support of a single communications link. Its main principle is based on transmitting digital data from a number of transmitters to a number of receivers within the same frequency band [8]. The MIMO principle is gaining importance in underwater applications, and one implementation is shown by Bouvet and Loussert in [8]. Quantification of the improvement obtained by using MIMO is shown in Bouvet's and Loussert's research. In addition, medium-range transmissions over shallow-water channels improve considerably with respect to a single-input single-output (SISO) approach. The spatial diversity of channels generated by multiple-antenna systems considerably lowers the probability that the transmitted waveform is attenuated due to destructive interference due to multipath. In Figure 2, an example of MIMO structure is shown. Multiple transmitting and receiving devices are shown in Figure 2.

Figure 2. Illustration of MIMO system structure (from [9]).

2. Modulation Scheme in Underwater Communications

It is well known that what limits the achievable data rate in a wireless communications system are bandwidth, the time spread of the channel which can cause ISI, and time variation of the channel due to Doppler spread effects. These issues are particularly important in acoustic communications systems in the water [10].

To transmit data most efficiently, a number of modulation techniques have been proposed. In particular, direct-sequence spread-spectrum (DSSS) systems are capable of resolving multipath propagation and exploiting delay diversity. In their research, Qu and Yang [11] developed a receiver with low complexity based on matched filtering, where multiple symbols are transmitted in each sequence period simultaneously. In addition, the high-reliable (HR) DSSS method provides both higher reliability and higher data rates. The high reliability and high rate are achieved with negligible self and co-channel interference [11].

Orthogonal Frequency-Division Multiplexing (OFDM) is another technique that has been gaining importance. Trung and Nguyen [10] analyze OFDM with MIMO by comparing the bit-error ratio (BER) performances for underwater communications. The main principle of this technique is based on dividing the bandwidth into subcarriers. The subcarriers are orthogonal to each other, and the processing is done by using fast Fourier transforms (FFT).

Simulation results in [10] show that the quality of signal transmission decreases from binary phase-shift keying (BPSK), quadrature phase-shift keying (QPSK), 16-quadrature amplitude modulation (QAM), and 16-phase-shift keying (PSK), respectively. This is due to the fact that when the modulation alphabet increases, the distance between points in the modulation constellation decreases. The decrease in the distance increases the likelihood of a wrong estimation of the signal. When Doppler shift causes a change in apparent frequency, it degrades the synchronization of the MIMO-OFDM system and the transmission quality as well [10].

Standard single-carrier modulation is still viable in underwater acoustic communications, provided the channel is well estimated and tracked. To initialize the receiver, a known training sequence can be inserted into the transmission. With this technique, ISI is reduced compared to the minimum mean-square error (MMSE) technique [12]. It is shown in the experiment results of [12] that BPSK and QPSK modulation techniques are effective and Doppler estimation of the channel works well in a long-range, shallow-water acoustic channel.

S. Kim, et al. [13] showed that by using a single-carrier modulation technique for shallow-water communications, channel bit-error rates in amplitude-shift keying (ASK) and BFSK can be on the order of 0.0088 and 0.0058 for a data rate of 1.0 kbps, respectively. They also showed that with QPSK modulation, the estimate of BER at 1.0 kbps is 0.0062, and the BER at 3.0 kbps is 0.0084. For the modulation techniques other than 16-QAM, it was shown that the experiment gave successful results with a BER on the order of 10^{-3} under normal environmental conditions [13].

3. Inter-symbol Interference Phenomenon and Channel Equalization

One of the effects of multipath in the channel is ISI. As illustrated in Figure 3, it is caused by the arrival of delayed copies of the signal. This causes the symbols to spread in time and overlap each other. Usually, this is remedied by channel equalization, which reduces the effects of ISI. There are different kinds of equalizers such as the linear equalizer, the decision-feedback equalizer, the blind equalizer, the turbo equalizer, the adaptive equalizer and the Viterbi equalizer [14]. In Figure 3, the dark-green line is the

first multipath arrival, which is typically the direct path between transmitter and receiver. The light green line is the second multipath, which arrives with some delay behind the first arrival and causes ISI.

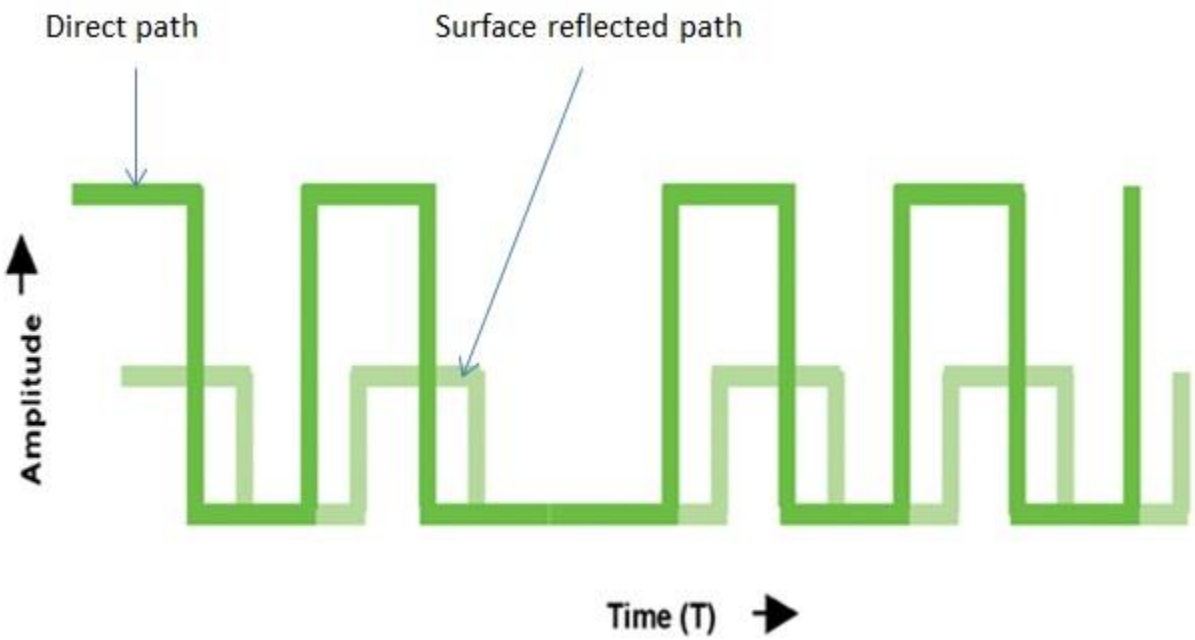

Figure 3. Illustration of inter-symbol interference (after [15]).

Zhong and Xiao-ling [16] compared some of the equalizer algorithms. According to their results, the decision-based feedback equalization (DFE) algorithms have better convergence in sparse multipath channels. Modified least mean squares (LMS) algorithms are more robust than the recursive least squares (RLS) algorithms in terms of convergence time. When the blind and adaptive algorithms are compared, it is shown that convergence is faster for the adaptive algorithm as compared to the blind algorithm. DFE algorithms were found to have very good phase tracking [16].

Another way of reducing the ISI effect in digital communications is to use a Kalman Equalizer Algorithm. The aim of this type of equalizer is to reconstruct the transmitted signal at the receiver. The tracking behavior of the Kalman equalizer with channel-coefficient estimation by LMS and RLS adaptive filters is compared in [17], and it is shown that Kalman equalization with RLS (K-RLS) has better performance than

Kalman equalization with LMS (K-LMS) in time-varying channels due to the rapid convergence of RLS in non-stationary environments.

THIS PAGE INTENTIONALLY LEFT BLANK

III. UNDERWATER ACOUSTIC CHANNEL AND COMMUNICATIONS

A. SOUND PROPAGATION

Sound propagates in a waveguide bounded by the sea surface and the sea floor in the ocean. Propagation of the sound is governed by the speed of sound, and rays refract toward regions of lower speed. Sound speed varies in the water according to the changing pressure, salinity, and temperature. Speed of sound can be expressed in terms of three independent variables: temperature T, salinity S, and depth z. It can be approximated as [18]:

$$c = 1449.2 + 4.6T - 0.055T^2 + 0.00029T^3 + (1.34 - 0.01T)(S - 35) + 0.016z \qquad (3.1)$$

where c is the speed of sound in meters per second, T is the temperature in Celsius, S is the salinity in parts per thousand, and z is the depth in meters.

Propagation of sound in the ocean can be modeled given the measured vertical sound-speed profile of the environment. According to ray theory, by using the launch angle of the ray and the speed of the sound at that depth, refraction is governed by Snell's Law,

$$\frac{\cos(\theta)}{c(d)} = const \qquad (3.2)$$

where θ is the horizontal angle of the ray and $c(d)$ is the speed of sound at depth d. The sound ray always bends toward the low sound speed region. For the sound-speed profile in Figure 4, the rays originating at a transmitter at depth $z = 9$ m follow the paths depicted in Figure 5. Refraction of rays towards regions of lower speed is exhibited in Figure 5.

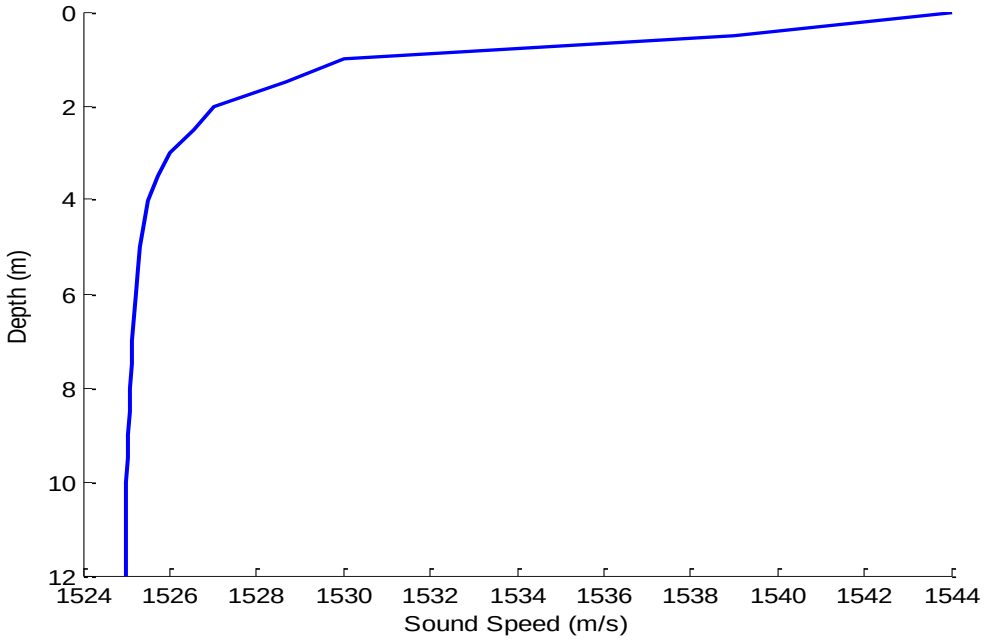

Figure 4. Measured sound-speed profile in a representative shallow-water channel.

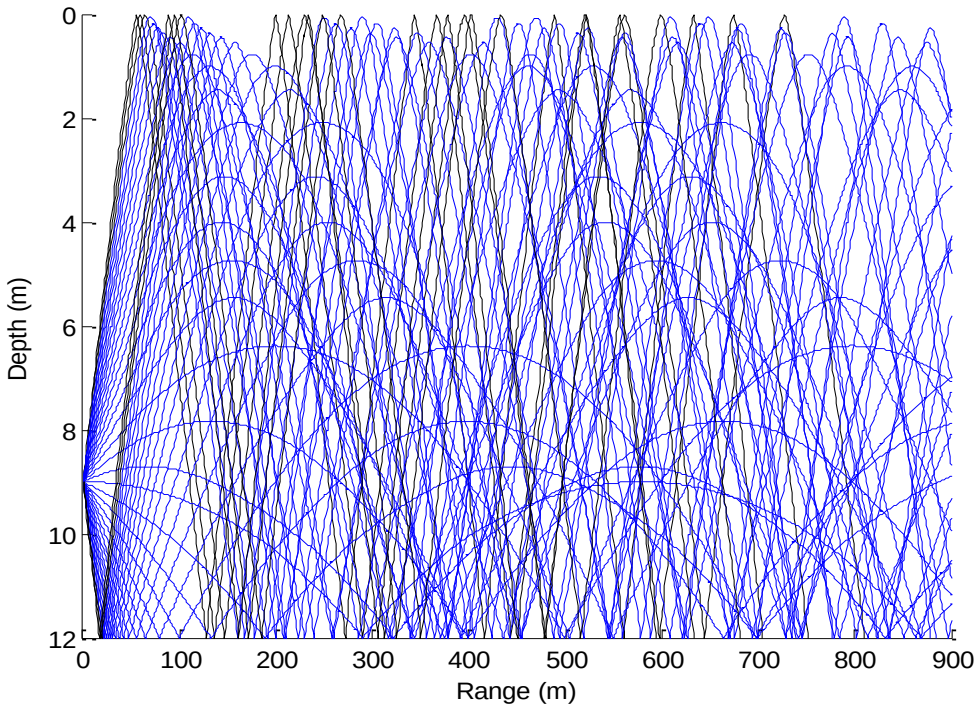

Figure 5. Illustration of the rays bending toward the lower speed of region in shallow water.

In underwater environments, there are two mechanisms that cause attenuation. The first one is geometrical spreading, and the second one is absorption by seawater. These mechanisms cause an intensity loss in the sound energy, and the term transmission loss (TL) is used to quantify it. TL is the ratio between the acoustic intensity $I(r)$ at the receiver location to the intensity $I(1)$ one meter away from the transmitter in dB [19]:

$$TL = 10\log_{10}\frac{I(r)}{I(1)} \text{ dB}. \tag{3.3}$$

Spherical spreading is dominant at closer distances, and the intensity of the sound is inversely proportional to the surface area of the sphere as

$$I(r) \propto \frac{1}{4\pi r^2}. \tag{3.4}$$

This situation can be visualized as a point source in a homogeneous medium, and the power radiated by the source is uniformly distributed over the surface area of the expanding sphere [1], [19].

For larger distances where the medium is bounded by sea surface and sea floor, cylindrical spreading approximates sound propagation. Intensity of the sound decreases with distance, so it is inversely proportional to the range in cylindrical spreading loss [19]. This relation can be stated as

$$I(r) \propto \frac{1}{r}. \tag{3.5}$$

The other mechanism that causes attenuation is absorption. Acoustic energy of the sound is absorbed as the sound propagates in the ocean. This depends on several factors like salinity, pH of water, temperature, pressure, and frequency. Additionally, sound is scattered by inhomogeneities, which contribute to the decay of sound intensity with range. It is hard to distinguish between absorption and scattering effects. Generally, both absorption and scattering increase as the frequency increases [18].

Transmission loss due to absorption and the frequency-dependent absorption coefficient are shown by

$$TL = ar \quad \text{dB}$$
$$a = \left(\frac{0.08}{0.9 + f^2} + \frac{30}{3000 + f^2} + 4\text{x}10^{-4}\right) f^2 \quad \text{dB/km} \tag{3.6}$$

where a is the absorption coefficient in dB/km and f is the frequency in kHz.

In Figure 6, the absorption coefficient in the units of dB/km is seen to be dependent on frequency.

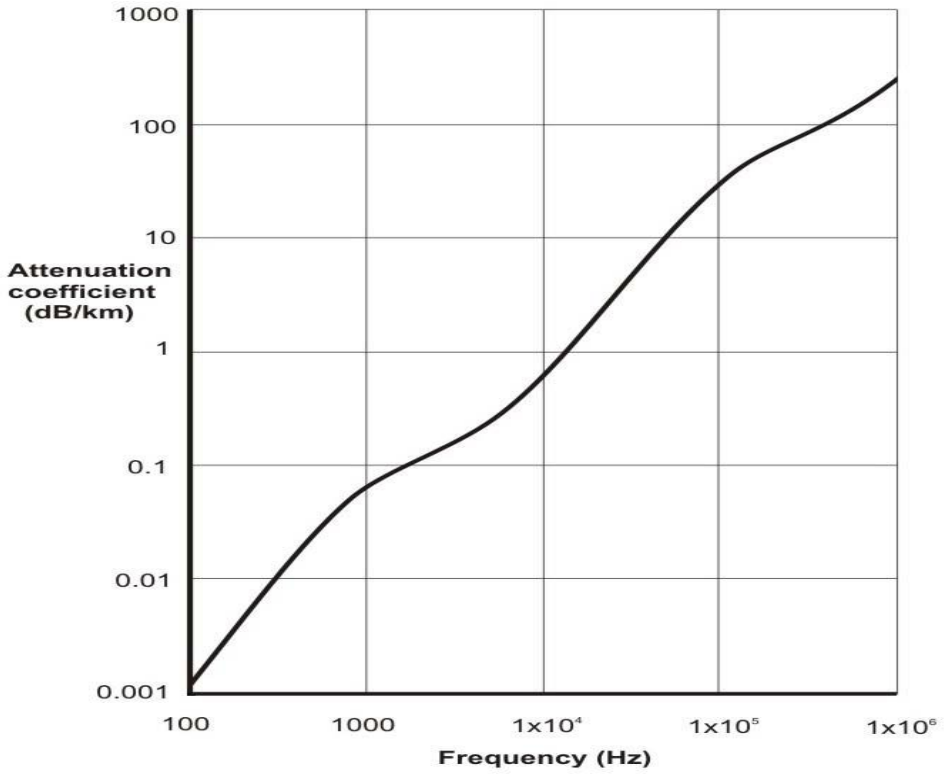

Figure 6. Absorption of sound in sea water at 20 C (from [20]).

B. NOISE IN THE OCEAN AND EFFECTS ON UNDERWATER COMMUNICATIONS

In addition to self-noise sources like electronic and thermal noises in the receivers, ambient noise limits the receiver capability in underwater communications [19].

Ambient noise is the noise in the environment at the receiver. At different frequencies, it depends on various factors like wind, wave actions, shipping, rainfall, marine animals, and seismic activities. For the frequency band of 20–30 Hz to a few hundred Hz, the dominant source of ambient noise is shipping activity. For the band of a few hundred Hz to 50 kHz, the frequency band for most acoustic modems, wave actions dominate. In this frequency interval, the noise depends on the wind and sea state as they affect the wave action. For the higher frequencies, thermal noise is the dominant source for an ambient noise [19], [21].

In the ocean, the ambient noise is not Gaussian and is represented as colored noise. On the other hand, for communications theory, it is standard to use additive white Gaussian noise (AWGN), whose power spectral density (PSD) is uniform over the range of frequencies [1].

C. MULTIPATH PROPAGATION IN THE UNDERWATER CHANNEL AND ITS EFFECTS ON COMMUNICATIONS

One of the most challenging underwater issues is multipath propagation. This phenomenon gives rise to frequency-selective fading in the acoustic channel due to destructive interference. The received signal is calculated by summing up the constant component and a random component that is time-varying in both phase and amplitude. The randomness of the signal can be described as [22]:

$$P(C) = Ce^{[-(C^2+D^2)/2]} I_0(CD) \tag{3.7}$$

where C is the sum of constant component and a random component which has unit variance on x and y coordinates, D is the absolute value of the constant coefficient, and $I_0(CD)$ is a modified Bessel function of zero order with argument CD. When there is

only a random component, D disappears and (3.7) reduces to a Rayleigh distribution function [22]:

$$P(C) = Ce^{[-(C^2)/2]} \ . \tag{3.8}$$

Acoustic transmission of the signal underwater is often characterized by Rayleigh fading, because the multipath structure of the underwater channel produces a random time-varying phase relationship [22], [23].

In underwater communications systems, the geometry of multipath propagation is very important because transmission to the receiver depends on the geometry of the source and receiver locations [24]. For the locations of the transmitter and the receiver, different paths are followed by the rays as illustrated in Figure 7.

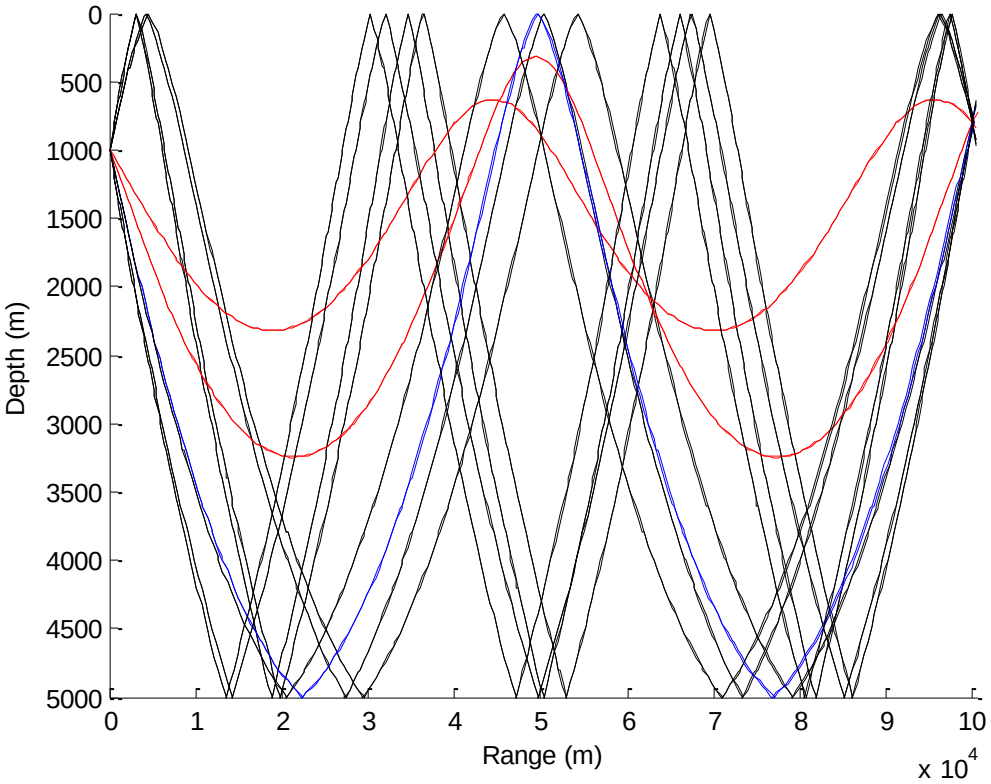

Figure 7. Different paths followed by the sound from the source positioned at 1000 m and the receiver positioned at 800 m for the 100 km long and 5000 m deep acoustic channel. (from [25]).

The rays follow the eigenpaths according to the sound-speed profile of the environment as governed by Snell's Law. In the waveguide environment of the acoustic channel, the locations of the source and receivers are very important. According to the relative positions of the source and receiver, multipath arrivals have variable delays, amplitudes, and phases.

Multipath propagation causes fading in the channel due to the different arrival times of the signals. Since they are following different paths, the resultant signal may widely vary in amplitude and phase. Multipath propagation causes two types of fading, flat fading and frequency-selective fading. Flat fading occurs when the delay spread is smaller than the symbol period. Frequency-selective fading occurs when the delay spread is larger than the symbol period or when the bandwidth is greater than the coherence bandwidth [14].

D. DOPPLER SPREAD IN THE UNDERWATER CHANNEL

The Doppler shift is a very important phenomenon in wireless communications and is caused by a relative velocity of either the ocean medium or the transmitter and receiver [1]. If there is no relative velocity, the received frequency is the same as the transmitted frequency. In this situation, there is no Doppler shift. If the distance between transmitter and receiver increases or decreases, the apparent frequency changes at the receiver. This condition causes the Doppler shift, a perceived change in frequency at the receiver relative to the transmitted frequency.

The expression for frequency of Doppler shift for the wave can be defined as

$$\Delta f_n = \frac{v}{\lambda} \cos \phi_n \tag{3.9}$$

where ϕ_n is the arrival angle at the receiver, v is the speed of the source, and λ is the wavelength of the signal.

Doppler spread is the result of time variations in the environment. It is related to Doppler shift and can be defined as the measure of frequency shift in the channel. Time

variations in the channel cause broadening of the spectral line [1]. Each multipath component has an associated Doppler spread. For example, the surface-reflected path usually has a larger Doppler spread than the direct path because of the variability caused by the rough and moving sea surface. Doppler spread D_s is simply approximated as

$$T_c \approx \frac{1}{D_s}. \tag{3.10}$$

where T_c is the coherence time, defined as the approximate time interval during which the channel is almost constant [14]. This definition is important because coherence time must be at least one symbol time long for successful processing.

In Figure 8, Doppler spread is seen to be the bandwidth of frequencies where the power spectrum is nonzero, and the value here is measured for the first path of the representative multipath channel. The dashed line in red color is a theoretical Doppler spectrum and the one with blue dots is a measured Doppler spectrum.

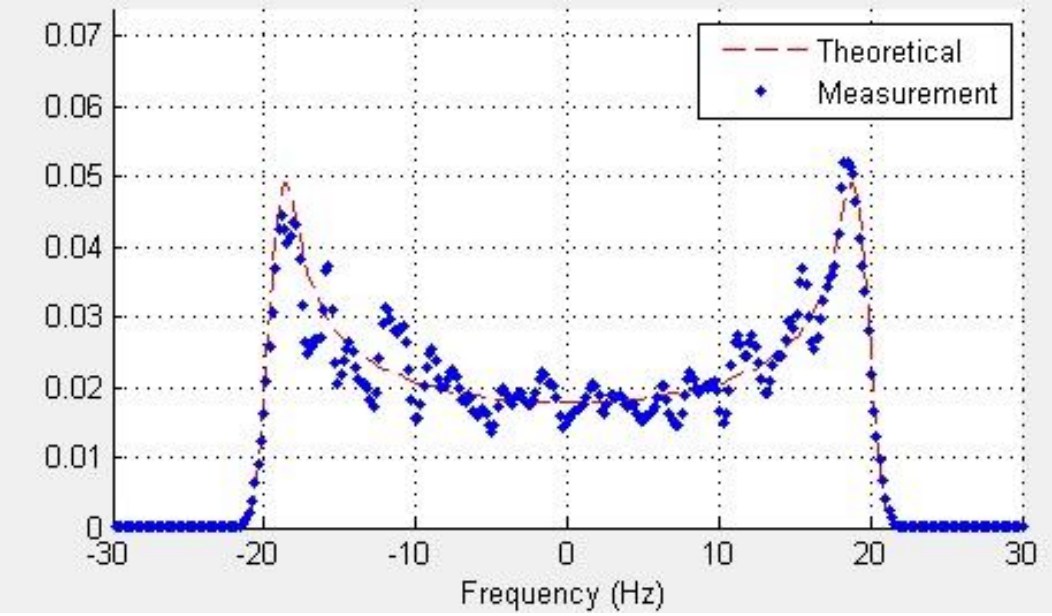

Figure 8. Illustration of Doppler spread for a measured value and a theoretical value for 20 Hz Doppler shift.

IV. BELLHOP RAY TRACING MODEL

A. MODEL DESCRIPTION

Bellhop is a beam tracing model that predicts and plots the acoustic field in the underwater environment. Porter and Bucker developed this algorithm in 1987 at the U.S. Navy Space and Naval Warfare Systems Center in San Diego [26]. In this thesis, the frequency range of 9-14 kHz is of interest, and Bellhop was selected because it is a reliable tool for frequencies greater than one kHz. Bellhop produces transmission loss, rays, eigenrays, arrival information, and graphs. Bellhop assumes that the bathymetry and properties of the ocean bottom do not change with range. The environment is represented as a two-dimensional vertical slice, containing both source and receiver. Reflection coefficients of the bottom and the surface can be specified in Bellhop [25], [26].

B. INPUT FILE

The Bellhop model requires an input file, which is called the environment file. The environment file is a simple text file and can be generated with any text editor. Basically, the environment file includes the sound-speed profile, the frequency of the signal, the number of receivers, source and receiver depths, ranges of the receivers to be measured, bottom and surface information, and the ray information including angles and number of beams. With this information, desired output files can be generated such as ray and eigenray plots, multipath arrival information, and transmission losses. In the input file, there are options for defining the surface and bottom characteristics, run types, and the units to be calculated. With the plot programs included in the Acoustic Toolbox [25] file, the desired output plots are obtained.

C. OUTPUT FILE

The output file is generated according to selected options. In this thesis, sound-speed profile plot, sound rays, eigenray plot, and impulse response plots are produced. First, the sound-speed profile of the environment is shown, and later, by selecting the ray-tracing option, the rays emanating from the source are generated. If the eigenray option is

selected, the rays that reach the specified receiver location are shown. After each tracing option is selected, the Bellhop program is run to make the calculations and produce the plot.

In Figure 9, possible inputs and outputs of the Bellhop ray tracing model are shown. Each file used as an input is run with Bellhop, and the output files or graphs are obtained according to the used run type methods of the input file.

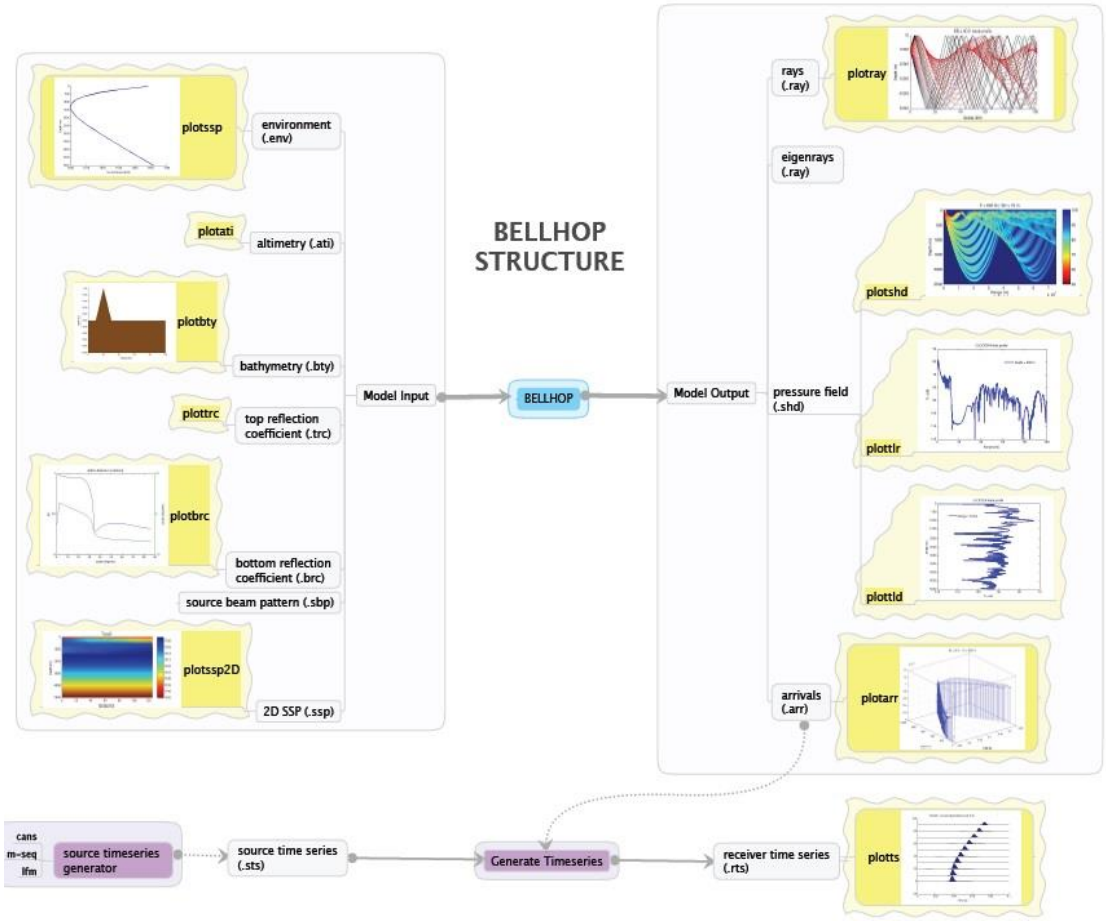

Figure 9. Bellhop model input and output structure (from [25]).

1. Ray Tracing Plot

After running the Bellhop program, **.prt** and **.ray** extended files are created and ray plots are obtained by using the appropriate command. The ray plot has the depth on the vertical axis and range on the horizontal axis according to the specifications in the environment file. The total fan of rays from the source is seen with different colors. The colors describe whether the ray reaches to the specified range directly or by reflecting from one boundary or both. A ray that has a red color defines a direct path from the source. It is usually the strongest path and usually is the first arrival. The blue colored rays have a reflection from one of the boundaries; these rays have less strength than the direct path. A black ray has multiple reflections between source and receiver and is usually the weakest of these three types [26]. An example of a ray trace plot is shown in Figure 10. For this representative plot, the depth of the channel is 12 m, and the transmitter is positioned at 9.5 m depth.

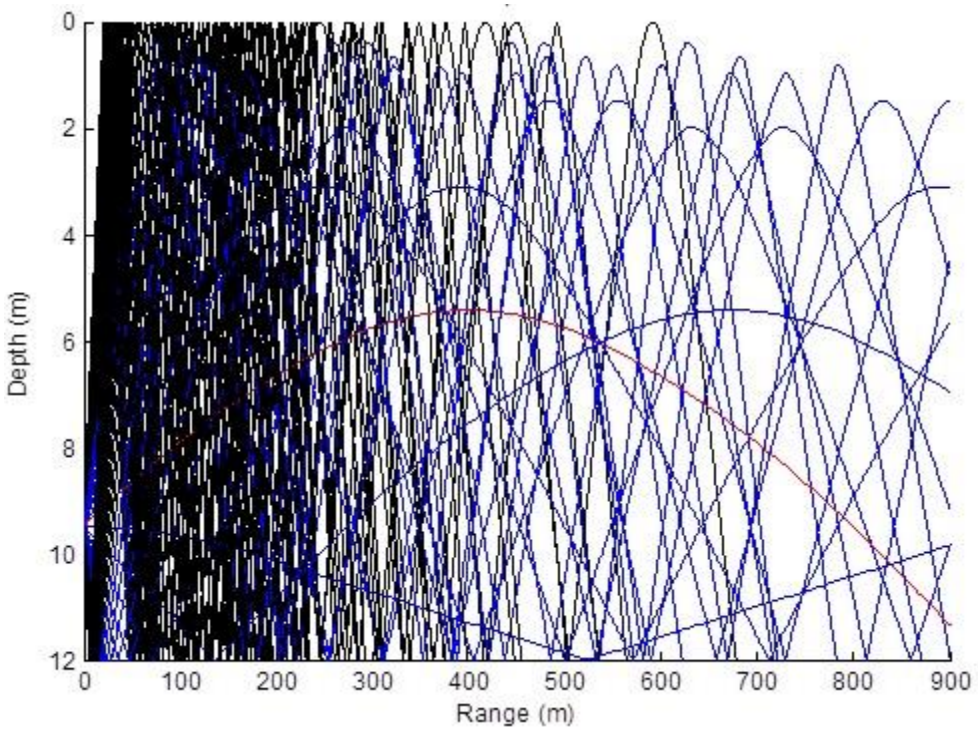

Figure 10. Ray trace plot for a 12 m deep acoustic channel.

2. Eigenray Plot

The eigenray plot shows the rays connecting the source to the specified receivers and has the same structure as the ray tracing plots. Depth of the channel is shown on the vertical axis, and the range is shown on the horizontal axis. All the multipaths (reflections and direct path) of the signal between source and receiver are displayed on eigenray plots. In Figure 11, eigenrays between the source at 9.5 m depth and receivers at 8 m and 10.5 m depth are illustrated for a horizontal range of 850 m.

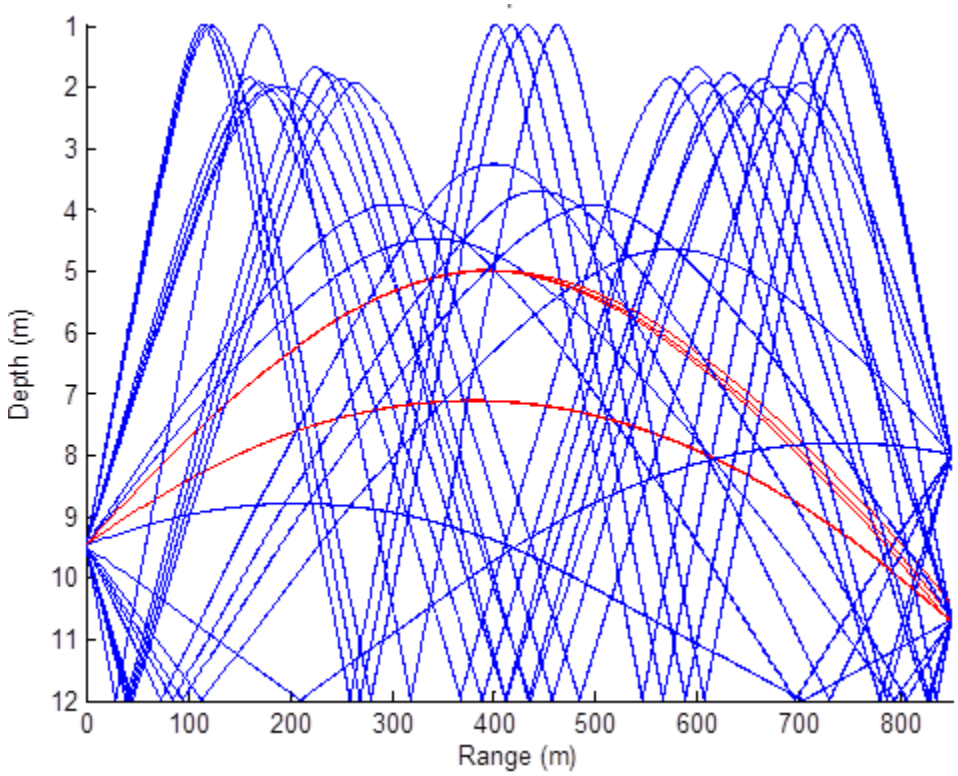

Figure 11. Eigenray plot for the receivers positioned at the depth of 8 m and 10.5 m for 12 m deep acoustic channel through the horizontal range of 850 m.

3. Impulse Response Plots

After running the program, an arrival file with the **.arr** extension is generated. This arrival file states the information about the number of the receivers and sources, receiver and source depths, channel frequency, amplitude and phase information of the arrivals, arrival times, bottom and surface reflection amounts, and launch and arrival

angles. In the impulse response plot, the amplitude of the impulse on the vertical axis is shown with respect to the arrival time on the horizontal axis. The amplitude of the impulse has no units. In Figure 12, it is seen that individual arrivals are at different times, and this difference is caused by the path length differences. The rays follow different paths and reach the receiver at different times.

The impulse responses generated by the Bellhop model represent the experimental underwater acoustic channel. For this modeled channel, the algorithms developed in the next chapter are tested.

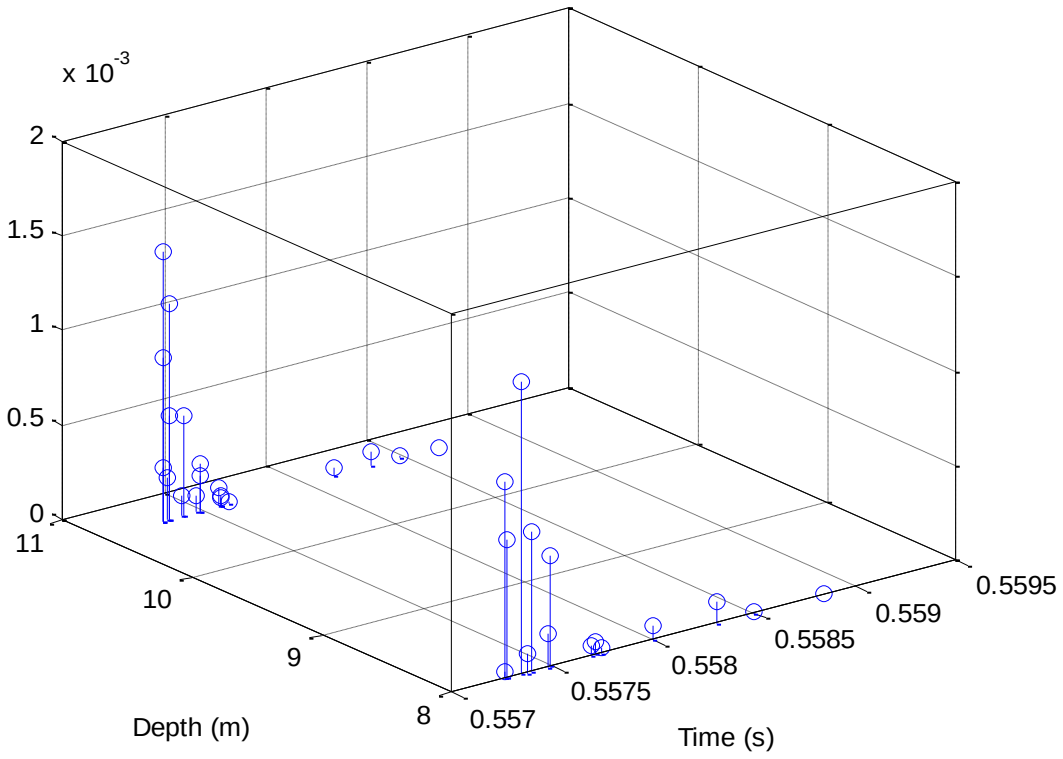

Figure 12. Impulse response plot when source is positioned at 9.5 m and the receivers are positioned at 8 m and 10.7 m depths with the horizontal range of 850 m away from the source.

THIS PAGE INTENTIONALLY LEFT BLANK

V. THEORETICAL BACKGROUND OF THE PROPOSED RECEIVER

A. MODULATION TECHNIQUE OF THE PROPOSED MODEL

In this thesis, a single-carrier QPSK modulation scheme is proposed for the communications system.

1. Phase-Shift Keying

In a standard single-carrier digital-communication system, the binary information may modulate the magnitude and phase of two sinusoidal signals of a given carrier frequency, with a phase difference of 90 degrees from each other such as a sine and a cosine signal as shown in Figure 13. This phase difference ensures orthogonality, which allows the in-phase and quadrature information from the two to be fully recovered at the receiver.

In single-carrier modulation, modulated signals are sent with the phase and amplitude information which is unique for each symbol and are represented by complex numbers. For complex representations of the modulated signals, this corresponds to a mapping of groups of bits into M -QAM symbols, where M usually takes the values 2, 4, 16, or 64. For example, the case of M equal to four, corresponds to 4-QAM (also called QPSK) as in Figure 14, which shows four possible values, called the "constellation."

In this method, each signal represents two bits. If the bit stream comes with a data rate of R bps, it is converted to the rate of $R/2$ symbols per second because signal elements represent two bits [14]:

$$\begin{aligned} s(t) &= A\cos\left(2\pi f_c t + \frac{\pi}{4}\right), && 00; \\ s(t) &= A\cos\left(2\pi f_c t + \frac{3\pi}{4}\right), && 01; \\ s(t) &= A\cos\left(2\pi f_c t - \frac{3\pi}{4}\right), && 11; \\ s(t) &= A\cos\left(2\pi f_c t - \frac{\pi}{4}\right), && 10. \end{aligned} \tag{5.1}$$

The QPSK transmitter block diagram is illustrated in Figure 13 and the QPSK constellation is illustrated in Figure 14.

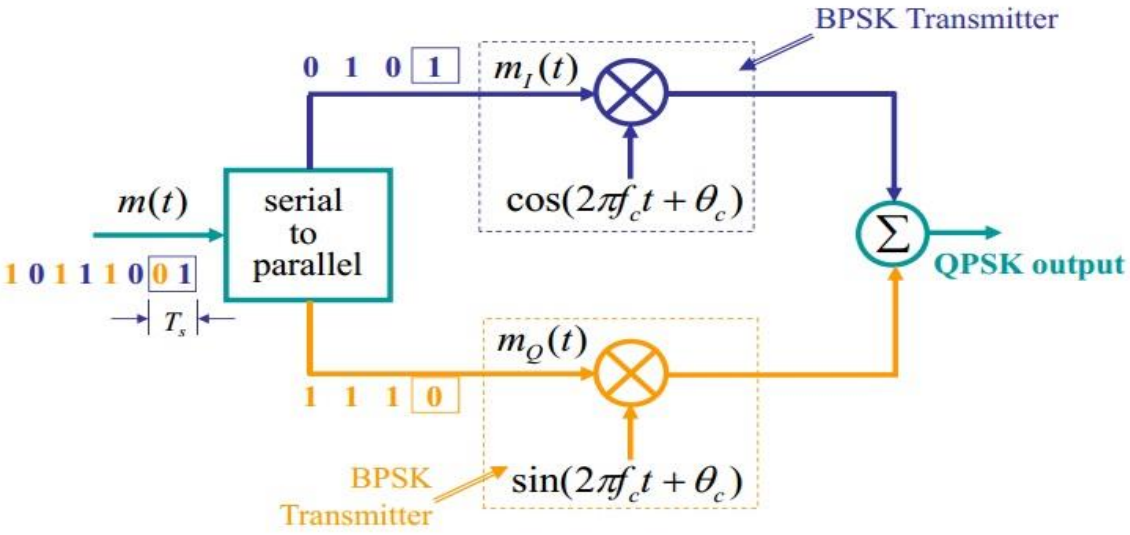

Figure 13. QPSK transmitter block diagram (from [14]).

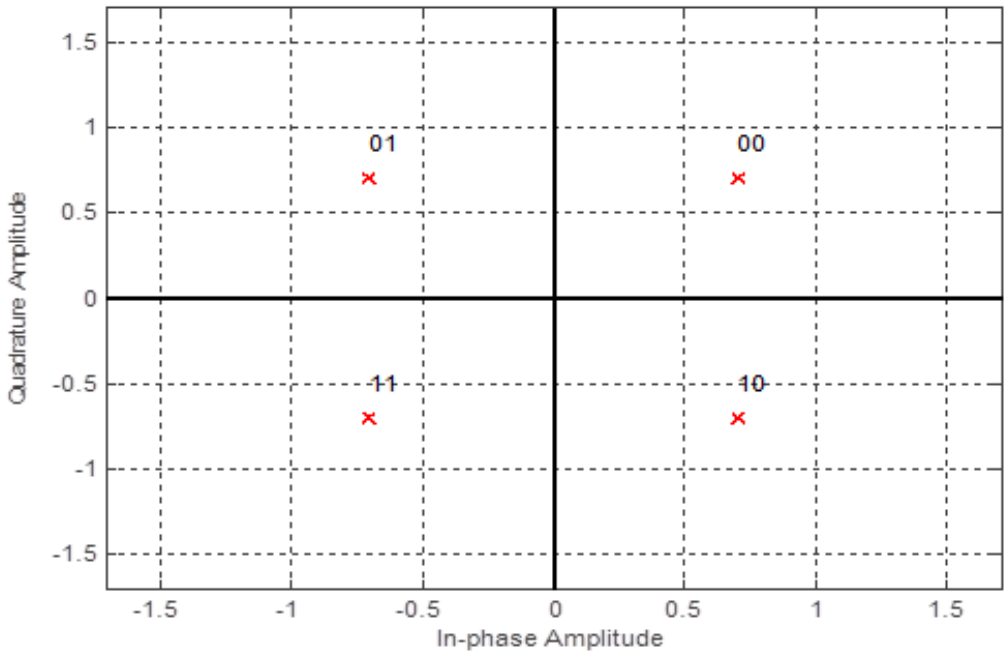

Figure 14. QPSK constellation of gray mapping with phase offset 0.7854 radians.

B. ERROR CORRECTION CODING

Noise and distortion in the communication channel invariably cause errors in the decoding of digital information. In order to cope with this problem, the information can be encoded so that errors can be detected and corrected. This is obtained by ECC, which adds extra bits to the transmitted message [27]. Forward error correction (FEC) is used in this research, specifically a convolutional encoding technique. This technique is used in systems that do not need complicated encoders, and the decoding performance exploits redundancy [27].

1. Forward Error Correction Coding

There are two basic types of FEC codes: block codes and convolutional codes. In this thesis, convolutional codes are used.

In a typical ECC system, for each k information data bits, n encoded data bits are transmitted, where $n > k$ [28]. Some of the encoding rates used are $1/2$, $2/3$, and $3/4$. In this thesis, a convolutional code rate of $1/2$ is used. In Figure 15, the block diagram of convolutional coding (CC) is illustrated. As shown, for every k input bits, n output bits are encoded.

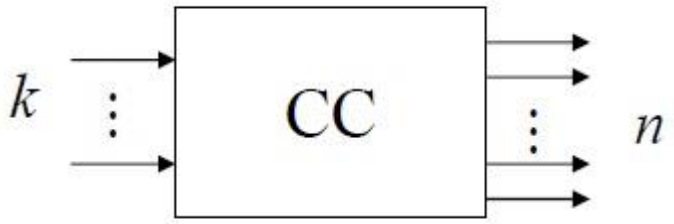

Figure 15. Convolutional coding with k data bits as an input and n coded bits as an output where $n > k$ (from [29]).

Since the number of symbols per second has to be the same, we can relate the data rate before and after the coder as

$$nT_{bc} = kT_b \tag{5.2}$$

where T_{bc} is the coded bit duration and T_b is the input data bit duration [28]. From this relation,

$$T_{bc} = \frac{k}{n} T_b = rT_b \tag{5.3}$$

and

$$R_{bc} = \frac{R_b}{r} \tag{5.4}$$

where R_{bc} is the bit rate of the coded data, R_b is the bit rate of the source data, and r is the code rate defined as [28]

$$r = \frac{k}{n}. \tag{5.5}$$

Convolutional encoding can be described in a number of different formats, including connection vectors or polynomials, the state diagram, the tree diagram, and the trellis diagram [27], [29].

A typical CC is defined in terms of binary convolution and implemented by tapped shift registers where each tap has a gain. For example, in Figure 16, for every bit of information x we have two encoded bits y_1 and y_2. The structure of convolutional code with a rate of $1/2$ is shown in Figure 16.

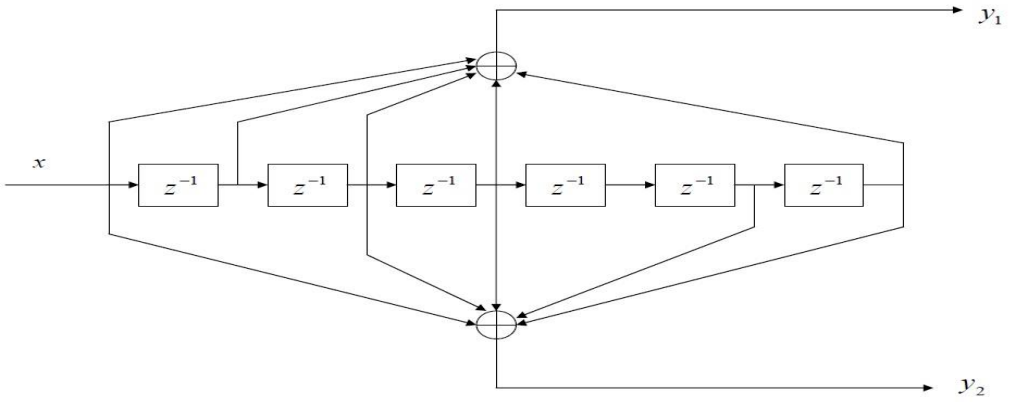

Figure 16. Convolutional encoding structure of code rate $1/2$ (from [29]).

The binary coefficients associated with the branches in Figure 16 can be grouped into octal numbers. In particular,

$$[y_1 \;\; y_2] = x[a_1 \;\; a_2] \tag{5.6}$$

where x describes the input of the structure, the vector a describes the coded connections between input and output, and the vector y describes the output of the structure [29]. For example, if the elements of a are given by

$$\begin{aligned} a_1 &= (1)_8(111)_8(001)_8 = 171 \\ a_2 &= (1)_8(011)_8(011)_8 = 133 \end{aligned}, \tag{5.7}$$

the code can be described by the matrix:

$$[y_1 \;\; y_2] = x[171 \;\; 133]. \tag{5.8}$$

2. Convolutional Decoding

The received sequence is compared with the possible transmitted sequences using the Viterbi algorithm. The Viterbi algorithm selects a maximum-likelihood path. When a valid path is selected, the input data bits are recovered from the corresponding output values [14].

C. CHANNEL ESTIMATION

As seen in the previous sections, channel multipath is responsible for ISI which, in turn, degrades the received signal. One of the remedies for this problem is to include channel equalization, which compensates for the channel spread.

This operation relies on knowledge of the impulse response of the channel, which in most cases is estimated using training sequences at the beginning of the transmission. Since, during the transmission, the channel most likely drifts with time due to motion and environmental conditions, estimates needs to be constantly updated so the effects of multipath are kept at minimum.

The main tool used for estimation is the well-known LMS algorithm, which recursively estimates the parameters of a linear model.

The channel response at the symbol rate is given by

$$y[n] = h[0]x[n] + h[1]x[n-1] + \cdots + h[N]x[n-N] + w[n] \tag{5.9}$$

where h values are the channel coefficients, and x is the transmitted sequence.

The LMS algorithm gives the estimated channel coefficients as

$$\hat{h} = \left[\hat{h}[0], \hat{h}[1], \ldots, \hat{h}[N] \right]. \tag{5.10}$$

At the beginning, $x[n]$ is known at the receiver, since it is the training sequence. When the data are transmitted, $x[n]$ is the demodulated data. This is the basis of the decision feedback equalizer, which we use for channel tracking.

The LMS adapts the channel estimates by minimizing the mean-square of the error signal. The error signal is the difference between the desired signal and the output of the filter [30]

$$e(n) = d(n) - \hat{d}(n). \tag{5.11}$$

In Equation 5.11, $e(n)$ is the error signal at time n, $d(n)$ is the desired signal, and $\hat{d}(n)$ is the output of the filter that is the current signal. First, the output signal is calculated by using the initial coefficient value. After finding the actual signal, Equation 5.11 is applied. This operation is done iteratively, and the filter coefficients are automatically updated [30].

One of the applications of adaptive filters is unknown system identification. The channel filter coefficients can be estimated with the LMS technique. The unknown system identification set-up is shown in Figure 17. The transmitted sequence is the input of both the channel and the adaptive filter. The desired signal is the output of the unknown system, and the adaptive filter converges to the coefficients of the unknown system with the LMS technique.

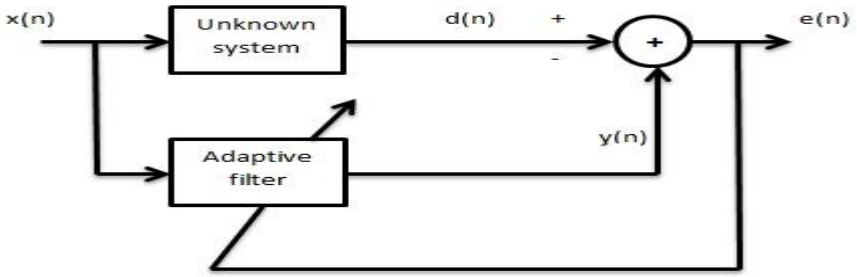

Figure 17. Unknown system identification set-up for adaptive filter (after [30]).

In this thesis, the input of the adaptive filter is the estimated sequence of the transmitted signal. The desired signal is applied to the adaptive filter with the delay because the system experiences a certain amount of delay in the FEC coding, modulation and the inverse process. The adaptive filter finds the optimal filter coefficients by converging to zero error. A schematic diagram of the proposed model is illustrated in Figure 18.

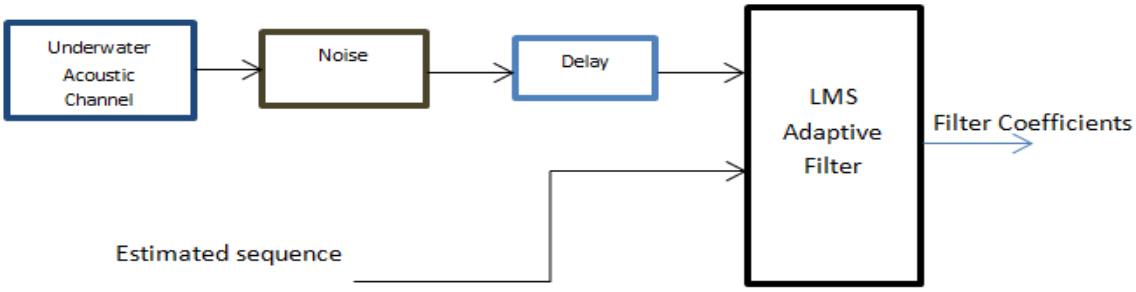

Figure 18. Illustration of the channel estimation in the proposed model.

D. EQUALIZATION USING ONE TRANSMITTER AND TWO RECEIVER ANTENNAS

The main contribution of this thesis is the investigation of the design of an optimal two-antenna receiver based on the well-known Kalman Filter technique. The key point is that in a single-input multi-output (SIMO) setting, the transmitted signal can be viewed as the state of a dynamic system, with the received signals being inputs and outputs. This result allows for the implementation of a technique that is not only

considered to be optimal under certain noise and linearity conditions but is also known to be robust and adaptable to a changing environment.

1. Kalman Filtering

The Kalman Filter is a well-known technique to compute the estimate of the state of a dynamic system subject to external disturbances. Under certain assumptions of linearity and white Gaussian disturbances, it provides an optimal estimate in the mean square sense. When some of these assumptions are relaxed, for example when the noise is not Gaussian, then the Kalman Filter is still the best linear estimator, and only a nonlinear filter can do better in terms of estimation error. The general equations for a linear system with external disturbances are

$$\begin{aligned} x(n+1) &= Ax(n) + Bu(n) + Gv(n) \\ y(n) &= Cx(n) + w(n) \end{aligned} \tag{5.12}$$

where $u(n)$ is the input signal, $y(n)$ is the output signal, $x(n)$ is the state, $v(n)$ and $w(n)$ are the uncorrelated white Gaussian noise sequences. Usually, the state $x(n)$ is a vector with dimensions larger than the dimensions of the input and output signals. The matrices $A, B,$ and C have appropriate dimensions and may also be time-varying, but they are independent of the input, output or state signals. The covariance of the two noise sequences Q and R are assumed to be known. In Figure 19, a standard setup of the linear stochastic dynamic model defined in (5.12) is illustrated.

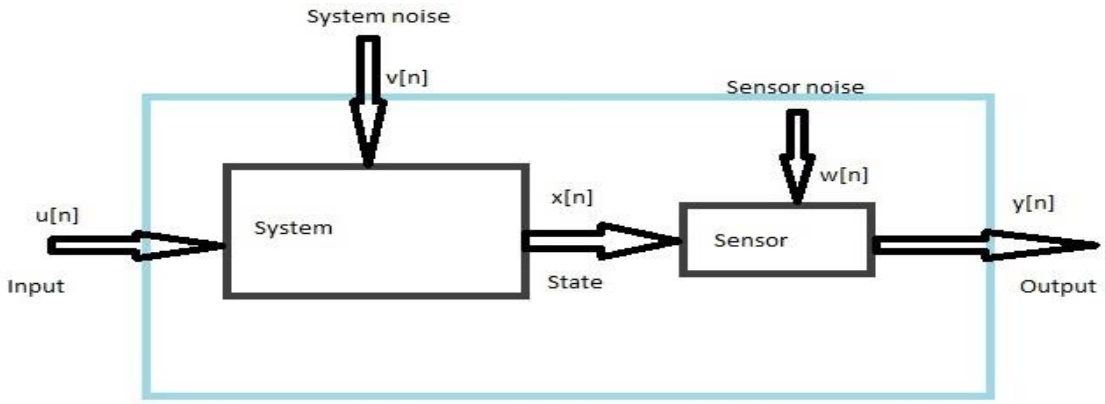

Figure 19. Linear stochastic dynamic model.

Under certain assumptions of observability, well documented in the literature [31], the state can be recursively estimated by the Kalman Filter, which alternates a prediction from the input signal $u(n)$ and a correction from the output signal $y(n)$.

In the next section, the case of one transmitter and two receivers is formulated using exactly the same model as in (5.12). The input and output signals $u(n)$ and $y(n)$ are actually the two received signals. In this way the state vector becomes an array of delayed versions of the transmitted signal. The role they play in the Kalman filter is that one of the signals becomes a predictor and the other a corrector, and this yields the best estimate of the transmitted signal embedded in the state vector. The whole technique requires the solution of a quadratic equation, called the Riccati Equation, dependent only on the dynamic model in (5.12).

2. Application to Two Antennas Demodulator

Let the transmitted data $x[n]$ be received by two receivers through two different channels as

$$\begin{aligned} y_1[n] &= h_{10}x[n] + h_{11}x[n-1] + \cdots + h_{1L}x[n-L] \\ y_2[n] &= h_{20}x[n] + h_{21}x[n-1] + \cdots + h_{2L}x[n-L] \end{aligned} \tag{5.13}$$

where the terms h_{ij} represent the impulse responses of the two channels which represent the arrivals of a transmitted impulse. The two channel impulse responses can be indicated in the vector form as h_1 and h_2 which are shown in (5.14) as

$$\begin{aligned} h_1 &= \begin{bmatrix} h_{10} & h_{11} & \cdots & h_{1L} \end{bmatrix} \\ h_2 &= \begin{bmatrix} h_{20} & h_{21} & \cdots & h_{2L} \end{bmatrix} \end{aligned} . \tag{5.14}$$

The received signals in both receivers can be found by the convolution of the transmitted signal and the channel impulse responses with additive noise,

$$\begin{aligned} y_1[n] &= h_1[n] * x[n] + w_1[n] \\ y_2[n] &= h_2[n] * x[n] + w_2[n] \end{aligned} \tag{5.15}$$

where w_1 and w_2 are the noise components in the channel. The covariance of the noise components are:

$$\begin{aligned} R &= E\left\{w_1(n)w_1(n)^T\right\} \\ Q &= E\left\{w_2(n)w_2(n)^T\right\} \\ N &= E\left\{w_1(n)w_2(n)^T\right\} = 0 \end{aligned} \tag{5.16}$$

where R, Q and N are the noise covariance.

The channel impulse responses are obtained from the Bellhop ray tracing model according to the given profile determined by environmental conditions as in Chapter IV. A typical channel impulse response is illustrated in Figure 20. In this example, the source depth is 10 m, the receiver depth is 7.5 m, and the receiver range is 770 m. It is clearly seen that the first signal arrival, which is probably the direct path between the transmitter and the receiver, has the greatest amplitude, and the other arrivals are decreasing in amplitude due to the reflections from the bottom and the surface of the ocean and the absorption attenuation.

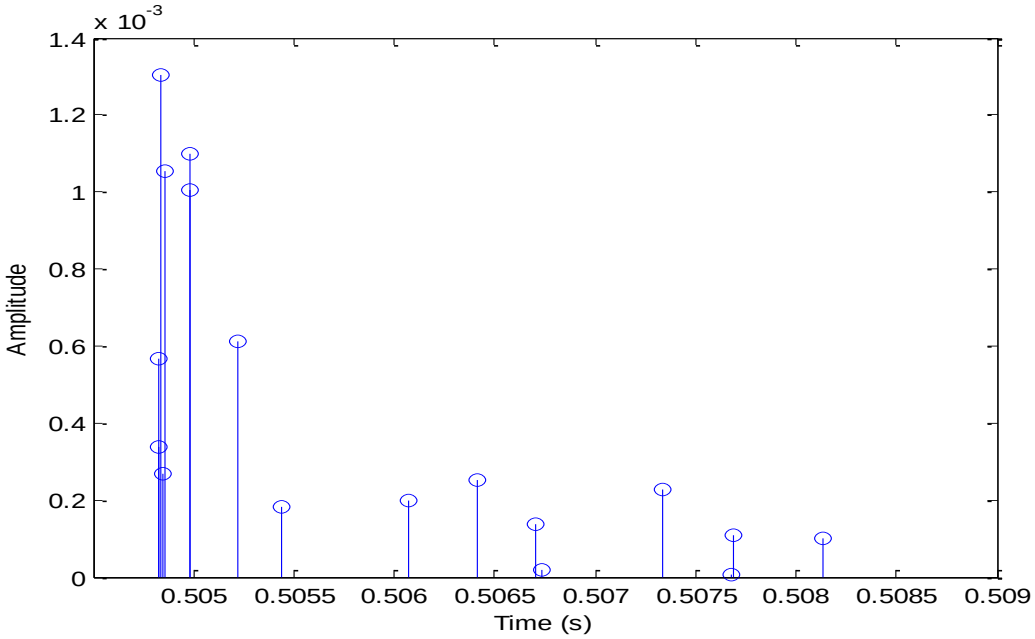

Figure 20. Illustration of the impulse response for 770 m long acoustic channel where the transmitter is positioned at the depth of 10 m and the receiver is positioned at the depth of 7.5 m.

The two impulse responses of the two acoustic channels are assumed to be estimated initially by the receiver using training sequences in the preamble. In Figure 21, the transmitted signal $x(n)$ and the received signals $y_1(n)$ and $y_2(n)$ through the two channels are represented as a block diagram.

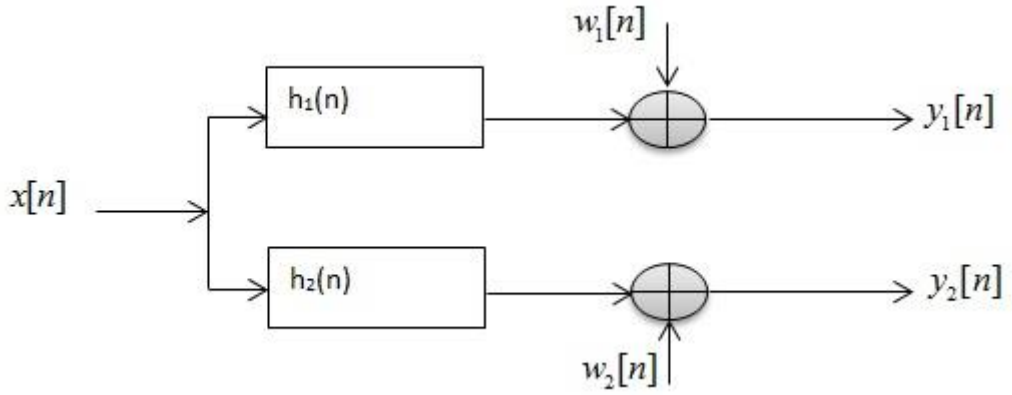

Figure 21. Illustration of the transmitted signal sent through two different acoustic channels with noise in the environment and the received signals (after [1]).

In what follows, it is shown that just by delaying one of the received signals, all signals in Figure 21 can be related by state space equations as (5.12) above. In fact, let

$$\begin{aligned} y_1[n] &= h_{10}x[n] + h_{11}x[n-1] + h_{12}x[n-2] + h_{13}x[n-3] + w_1[n] \\ y_2[n] &= h_{21}x[n-1] + h_{22}x[n-2] + h_{23}x[n-3] + w_2[n] \end{aligned} \tag{5.17}$$

where, for simplicity, we used a third order system. Then $x[n]$ can be written in the following form:

$$x[n] = \frac{1}{h_{10}}(y_1[n] - h_{11}x[n-1] - h_{12}x[n-2] - h_{13}x[n-3] - w_1[n]). \tag{5.18}$$

Define the state vector as

$$\underline{x}[n] = \begin{bmatrix} x[n-1] \\ x[n-2] \\ x[n-3] \end{bmatrix}. \tag{5.19}$$

The goal is to define the state and estimate the past sequences of the transmitted signal vector $\underline{x}$. It can be easily verified that:

$$[0,\cdots,1]\begin{bmatrix} x[n-1] \\ \vdots \\ x[n-N] \end{bmatrix} = x[n-N]. \tag{5.20}$$

Equations (5.17), (5.18), and (5.19) can be combined in the following form:

$$\begin{bmatrix} x[n] \\ x[n-1] \\ x[n-2] \end{bmatrix} = \begin{bmatrix} -h_{11}/h_{10} & -h_{12}/h_{10} & -h_{13}/h_{10} \\ 1 & 0 & 0 \\ 0 & 1 & 0 \end{bmatrix}\begin{bmatrix} x[n-1] \\ x[n-2] \\ x[n-3] \end{bmatrix} + \begin{bmatrix} 1/h_{10} \\ 0 \\ 0 \end{bmatrix} y_1[n] - \begin{bmatrix} -1/h_{10} \\ 0 \\ 0 \end{bmatrix} w_1[n]$$
$$y_2[n] = \begin{bmatrix} h_{21}[n] & h_{22}[n] & h_{23}[n] \end{bmatrix}\begin{bmatrix} x[n-1] \\ x[n-2] \\ x[n-3] \end{bmatrix} + w_2[n] \tag{5.21}$$

The two equations in (5.21) yield the state space model of the received signals y_1 and y_2. Equation (5.21) can be related to the general equations depicted in (5.12) and is shown as:

$$A = \begin{bmatrix} -h_{11}/h_{10} & -h_{12}/h_{10} & -h_{13}/h_{10} \\ 1 & 0 & 0 \\ 0 & 1 & 0 \end{bmatrix}, B = \begin{bmatrix} 1/h_{10} \\ 0 \\ 0 \end{bmatrix}, G = \begin{bmatrix} -1/h_{10} \\ 0 \\ 0 \end{bmatrix}, C = \begin{bmatrix} h_{21} & h_{22} & h_{23} \end{bmatrix}. \tag{5.22}$$

The general equations of the Kalman Filter in (5.12) can be written in the following form as the model in this thesis:

$$\begin{aligned} \underline{x}(n+1) &= A\underline{x}(n) + By_1(n) + Gv(n) \\ y_2(n) &= C\underline{x}(n) + w(n) \end{aligned}. \tag{5.23}$$

We see from (5.23) that the actual states and the Kalman estimator algorithm estimates the state by making prediction and corrections. Measurement updates for the Kalman estimator are

$$\underline{\hat{x}}[n|n] = \underline{\hat{x}}[n|n-1] + M(y_2[n] - C\underline{\hat{x}}[n|n-1]) \tag{5.24}$$

where $\underline{\hat{x}}[n|n]$ is the updated estimate at time n and $\underline{\hat{x}}[n|n-1]$ is the estimate of the transmitted sequence $\underline{x}[n]$ with the previous time measurements. The symbol M refers to the innovation gain matrix.

$$\underline{\hat{x}}[n+1|n] = A\underline{\hat{x}}[n|n] + By_1[n]. \tag{5.25}$$

Equation (5.25) addresses the time update of the estimator algorithm. The quantity $\underline{\hat{x}}[n+1|n]$ is the one-step ahead predictor that estimates the state value at the next time sample by using the current estimate $\underline{\hat{x}}[n|n]$. Substituting (5.24) into (5.25) gives

$$\underline{\hat{x}}[n+1|n] = A\underline{\hat{x}}[n|n-1] + By_1[n] + K(y_2[n] - C\underline{\hat{x}}[n|n-1]) \tag{5.26}$$

where $K = AM$ is the Kalman gain matrix.

Equation (5.25) and the actual state can be modified in order to have an expression for error covariance matrix. State error is the difference between the actual state and the predicted state and can be defined as

$$\underline{\tilde{x}}[n] = x[n] - \hat{x}[n]. \tag{5.27}$$

Error covariance matrix for the state is

$$P(n) = E\left\{\underline{\tilde{x}}[n]\underline{\tilde{x}}[n]^T\right\} \tag{5.28}$$

where $P(n)$ is the notation for covariance. By using (5.25) and the actual state, we obtain the error covariance matrix

$$P[n+1|n] = AP[n|n]A^T + Q. \tag{5.29}$$

The Kalman filter computes the state estimate in terms of predictor and corrector. Using the Bayesian linear estimation and the relationships illustrated in the equations above, we get

$$\underline{\hat{x}}[n+1|n] = A\underline{\hat{x}}[n|n-1] + By_1[n] + K(n)(y_2[n] - C\underline{\hat{x}}[n|n-1]),$$
$$K(n) = P[n|n-1]C^T(CP[n|n-1]C^T + R), \tag{5.30}$$
and
$$P[n+1|n] = AP[n|n-1]A^T - AP[n|n-1]C^T(CP[n|n-1]C^T + R)^{-1}CP[n|n-1]A^T + Q\ .$$

The Riccati Equation gives recursive results by starting with an initial value of the covariance matrix. Impulse responses of two different channels are used as an initial value to form the matrices and solve the Riccati Equation which gives the state filter coefficients.

In a steady-state implementation, this estimator results in the superposition of the output of two filters as shown in Figure 22.

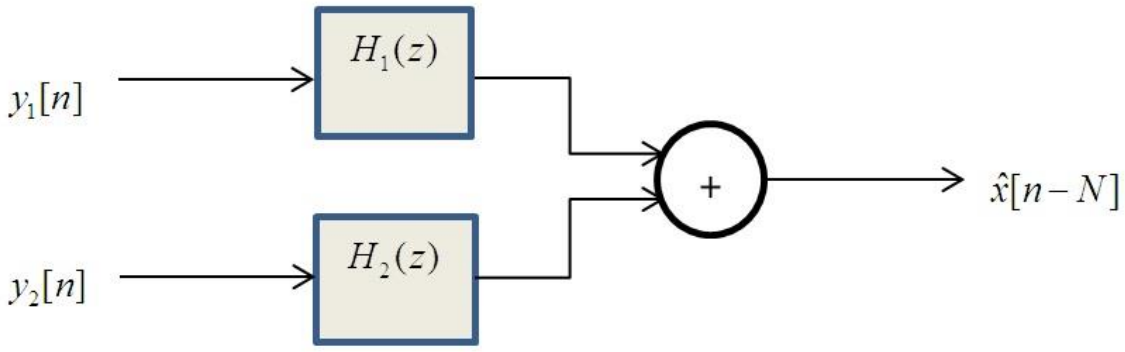

Figure 22. Block diagram representation of Kalman state filters (after [1]).

The state filter coefficients are always updated by the estimated values. By summing up two digital state filters, the estimation of the transmitted sequence is obtained.

VI. SIMULATION RESULTS

A. SHALLOW-WATER ACOUSTIC CHANNEL

To test the proposed system in a realistic environment, an artificial channel is created in the Bellhop ray tracing model. In the created shallow-water channel, some different measurements are taken to show the channel estimation quality by using the estimated sequence of the transmitted data as an input signal to the LMS adaptive filter.

In the simulated acoustic channel, the depth is assumed to be 12.5 m, and there is an assumption of a temperature-driven gradient in the environment. The sound-speed profile of the artificial channel is shown in Figure 23. The speed of sound decreases sharply in the first two meters and then it decreases gradually.

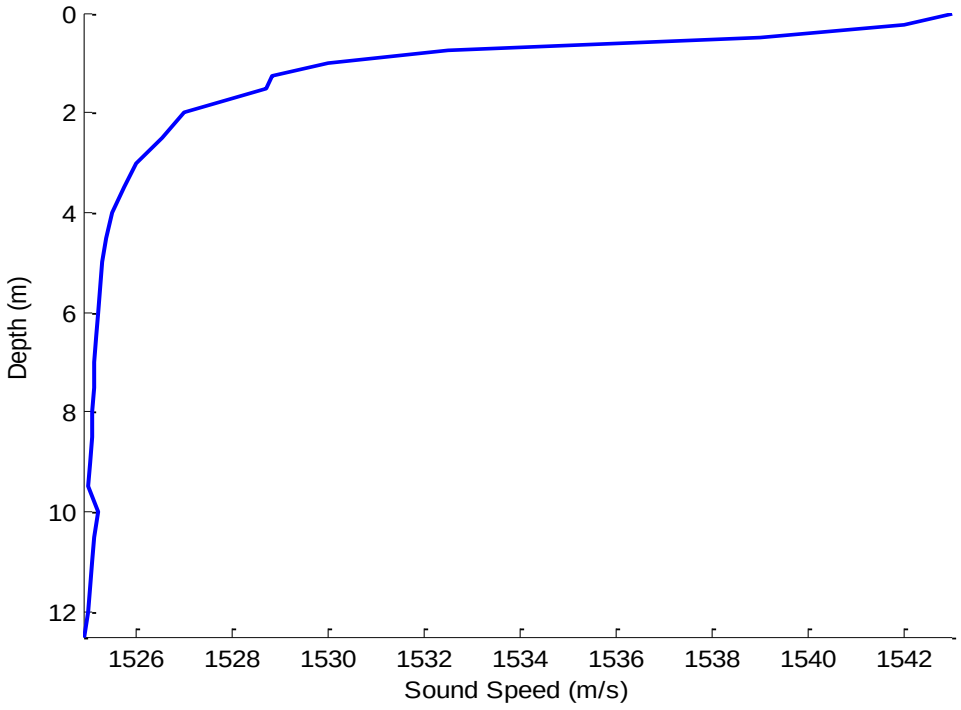

Figure 23. Sound-speed profile of the shallow-water artificial channel.

The horizontal distance between the transmitter and the receiver is selected as 960 m. The transmitter is at a depth of 10 m, and the receivers are put at depths of 9.5 m 11.5 m. Bottom type is assumed as sand-silk-clay, which has fairly high compressional wave attenuation. Sea state is assumed to be zero, and the depth of the channel is range-independent between the transmitter and the receiver.

Multiple propagating paths from the given source are illustrated in Figure 24. There are both the direct path that is shown in red and reflected paths that are shown with blue and black colors to a maximum range of 1100 m. Even the direct path, which is reflected by neither the bottom nor the surface, does not propagate on a straight line due to the sound-speed gradient in the water column.

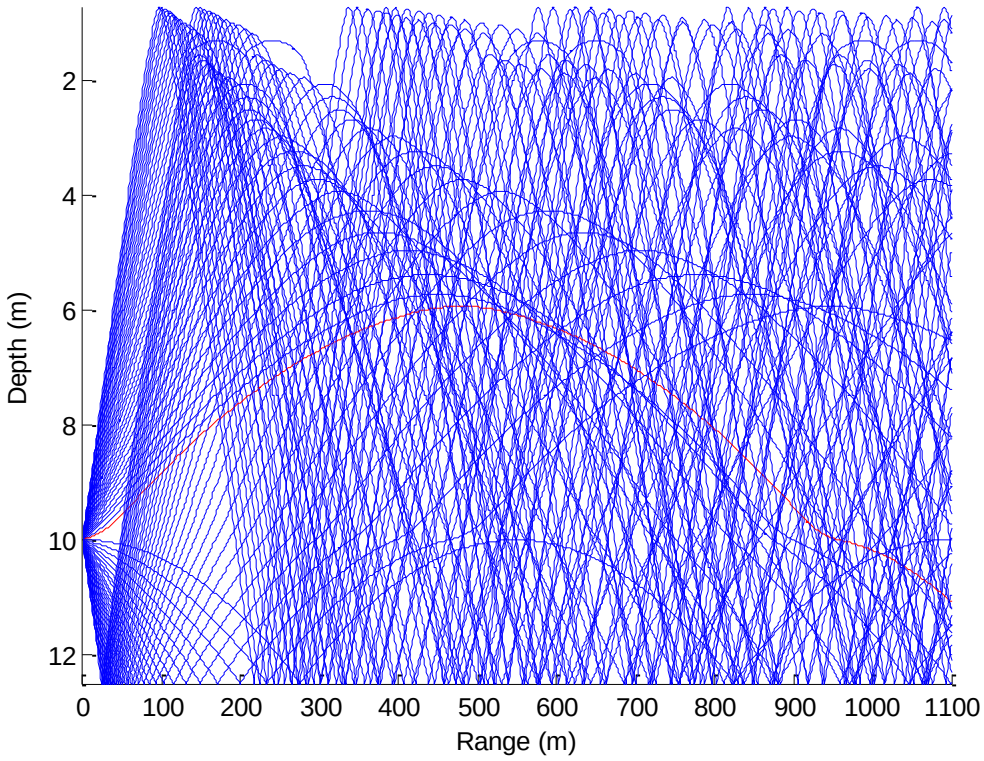

Figure 24. Illustration of emanating rays from the source at 10 m in shallow-water acoustic channel.

Depending on where a receiver is positioned, only a subset of propagating rays reach it. To see the rays reaching the receivers, an eigenray plot is exhibited in Figure 25. There are direct paths for both receivers.

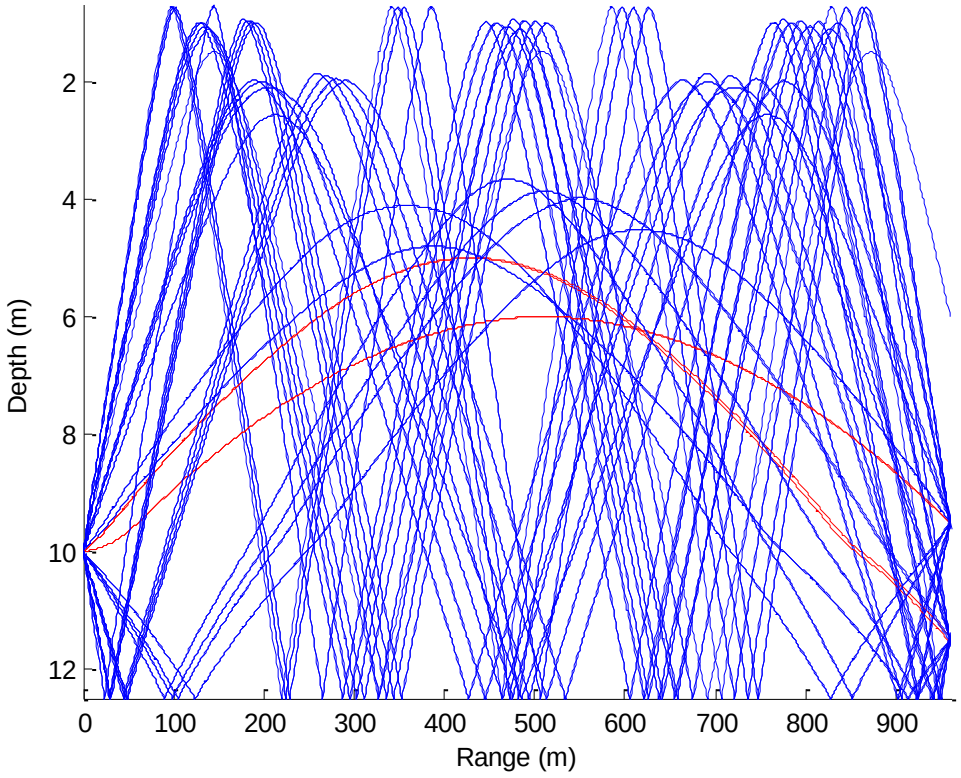

Figure 25. Illustration of eigenrays when the transmitter is positioned at a depth of 10 m and the receivers at depths of 9.5 m and 11.5 m in the 12.5 m deep acoustic channel.

To extract detailed information about the arrival signals, impulse response plots for both receivers are produced. From these impulse response plots, amplitude, phase, and arrival time information are used in representation of the Rayleigh fading channel in Simulink. Channel impulse responses for both receivers are illustrated in Figure 26 and 27.

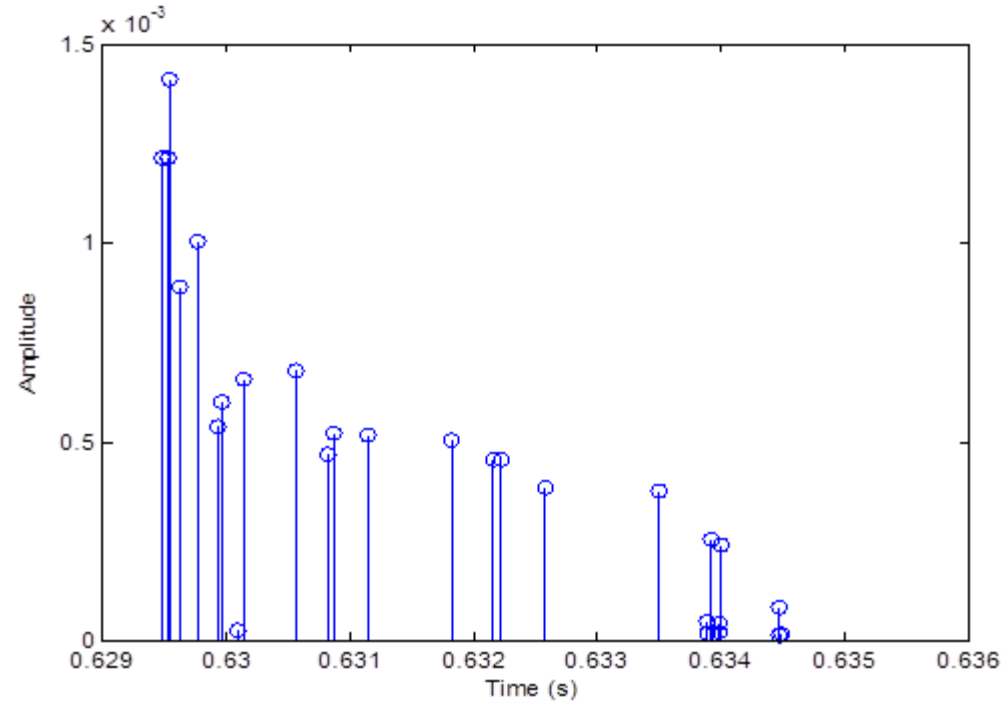

Figure 26. Arrivals with the receiver positioned at a depth of 9.5 m and the transmitter positioned at 10 m in shallow-water acoustic channel.

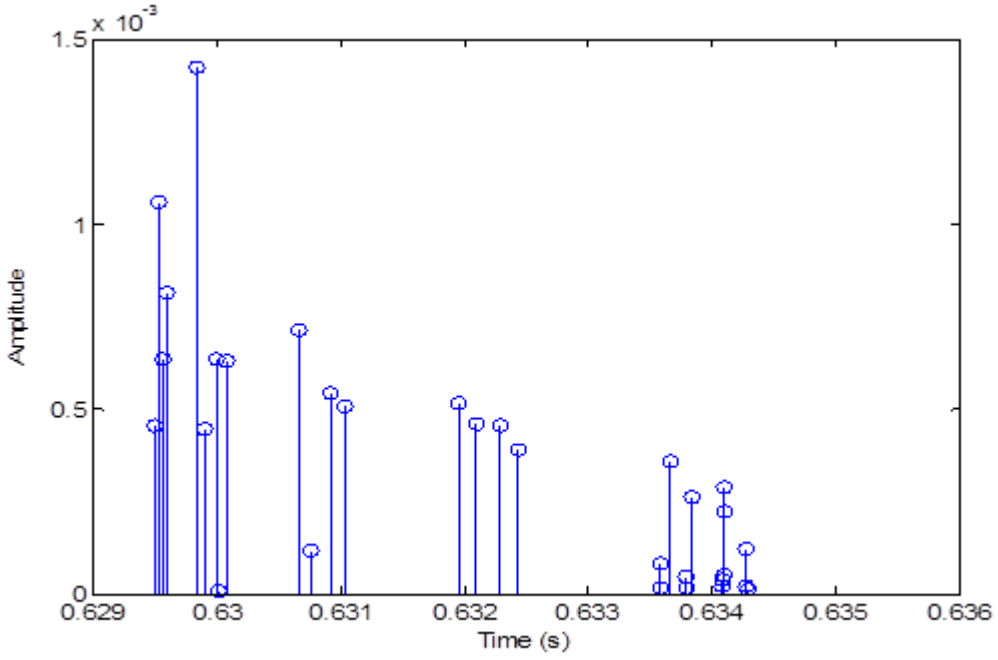

Figure 27. Arrivals with the receiver positioned at a depth of 11.5 m and the transmitter positioned at 10 m in shallow-water acoustic channel.

It is clearly seen in Figures 26 and 27 that there are groups of arrivals at different times. Each group of arrivals is approximated to one arrival value by using the phase and amplitude information, and the time is averaged for each group. The total arrived signal power is calculated in dB to use in the Rayleigh fading channel model.

The signal is disturbed by AWGN, and the measurements are taken from zero dB to 36 dB to see the channel estimation quality. For each of the AWGN values, the simulation was run a large number of times to obtain consistent results. The sampling time for the source data was selected as $1/2000$ seconds, and the symbol rate was 1000 symbols/second. An increase in the symbol rate causes more calculations for the Kalman state filters. A code rate of $1/2$ was used in ECC section. In the error-decoding part, a hard decision technique was applied. In the channel estimation part, a normalized LMS technique was chosen, and step size 0.2 was used for calculations.

The same measurements were taken for two different Doppler shift values. Doppler shift frequencies of 1.0 Hz, and 0.1 Hz were used to compare the channel estimation quality for two different channel variabilities. To show the relative differences between error values as a function of signal-to-noise ratio (SNR), the magnitude of the results were normalized to one. Normalized-error magnitude values are illustrated in Figure 28. The error rate for Doppler shift 1.0 Hz is larger than Doppler shift 0.1 Hz. Another important result which can be deduced for a Doppler shift of 1.0 Hz is that the error converges to a value that does not change much above some certain SNR value, but for a Doppler shift of 0.1 Hz, the error keeps decreasing up to a SNR of 36 dB. For smaller SNR, there is not much difference between 1.0 Hz and 0.1 Hz, but as the SNR increases, the difference between the errors for a Doppler shift of 1.0 Hz and a Doppler shift of 0.1 Hz increases.

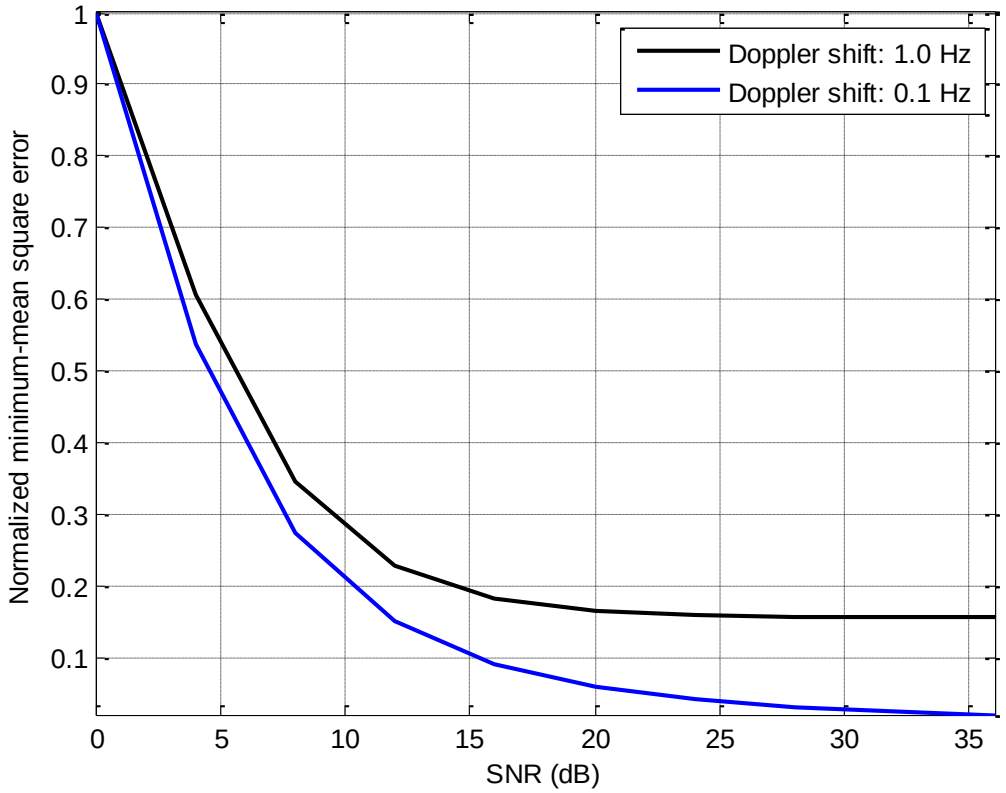

Figure 28. Normalized minimum-mean square error of channel coefficients in representative shallow-water acoustic channel.

Another important observation related to this system is that at lower Doppler shift frequencies such as 0.1 Hz, the estimated channel coefficients can calculate the transfer function and recover the transmitted sequence with zero error, but for relatively a large Doppler shift such as 1.0 Hz, the error converges to a constant value so that the estimated channel coefficients are too noisy to calculate the transfer function and recover the transmitted data signal without error.

Percent error rate for the channel estimation was calculated, and the results are depicted in Figure 29. When the Doppler shift is 0.1 Hz, the percent error approaches zero for larger SNR. On the other hand, when the Doppler shift frequency is 1.0 Hz, the percent error is higher, and this error rate affects the calculation of Riccati equation by using estimated channel coefficients.

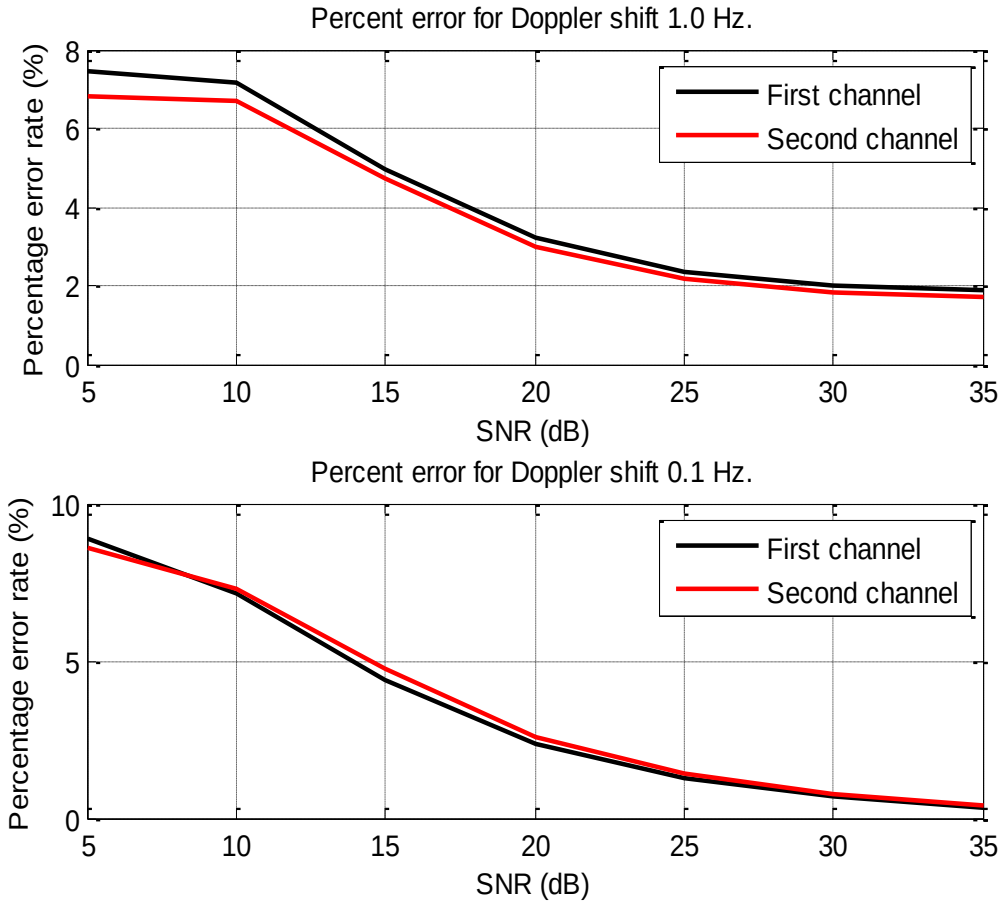

Figure 29. Percent-error rate of channel estimation in the artificial shallow-water channel.

B. DEEP-WATER ACOUSTIC CHANNEL

The second scenario is chosen to be a deep-water channel, and a measured Kauai sound-speed profile was used for the environment. The Kauai sound-speed profile is shown in Figure 30.

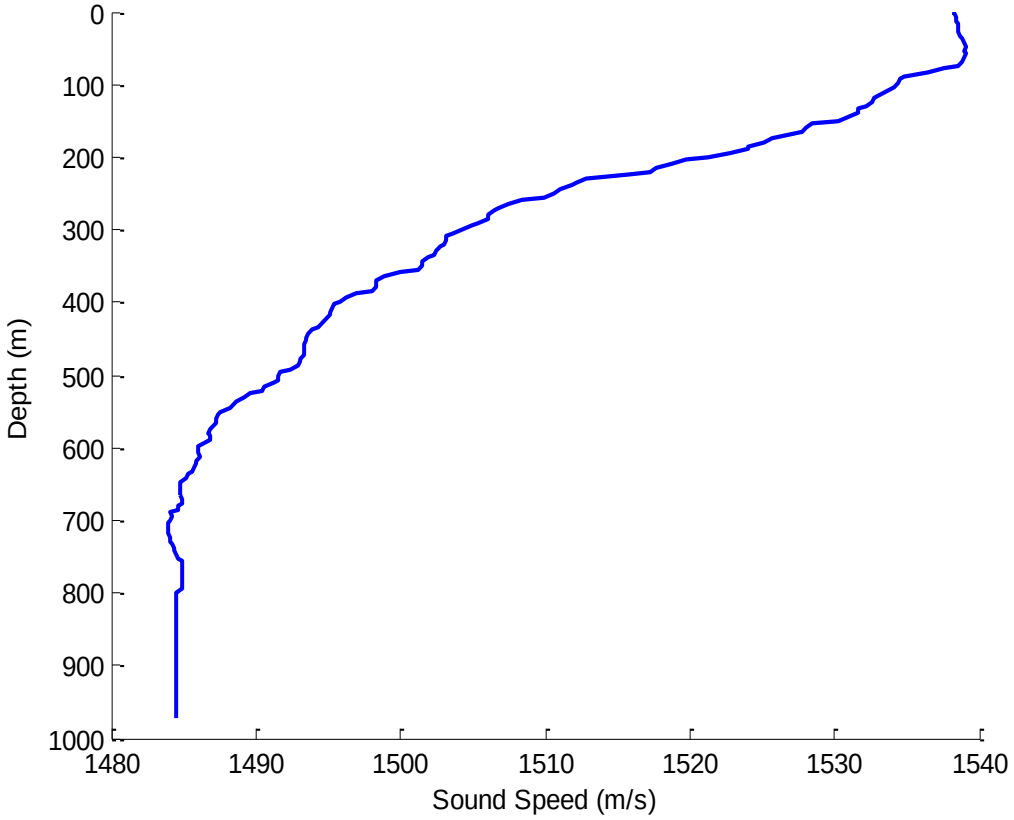

Figure 30. Kauai, HI environment sound speed profile (from [25]).

As seen in Figure 30, the Kauai environment has a positive gradient up to depths 55-60 m and after these depths has a negative gradient. After around 650 m, the environment is almost isospeed.

The source is assumed to be at 920 m depth for this case, and the receivers are close to the surface at depths of 5 m and 23 m. The horizontal range between source and the receivers is 5000 m, and the bottom type is identified as silt. Sea-state is assumed to be zero. For these conditions, the rays emanating from the transmitter at 920 m depth are depicted in the ray tracing plot in Figure 31. The beam angle extends from -25 degrees to 25 degrees.

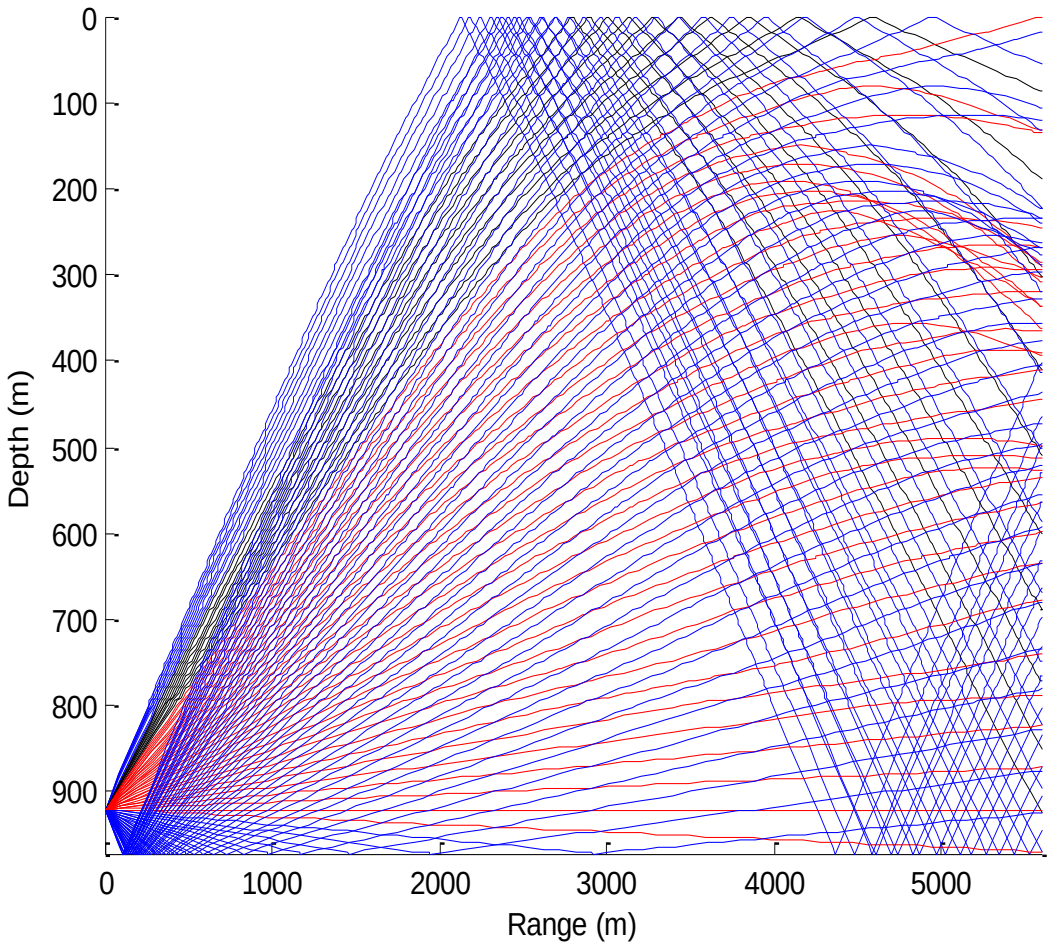

Figure 31. Illustration of emanating rays from the source at 920 m in Kauai, HI environment.

To see the rays arriving at the specific receiver locations, the eigenray plot is used, and to see the specific information related to each eigenray, the arrivals file and impulse response plots are generated. The eigenray plot is shown in Figure 32, and the impulse response plots for two receivers are shown in Figure 33 and Figure 34, respectively.

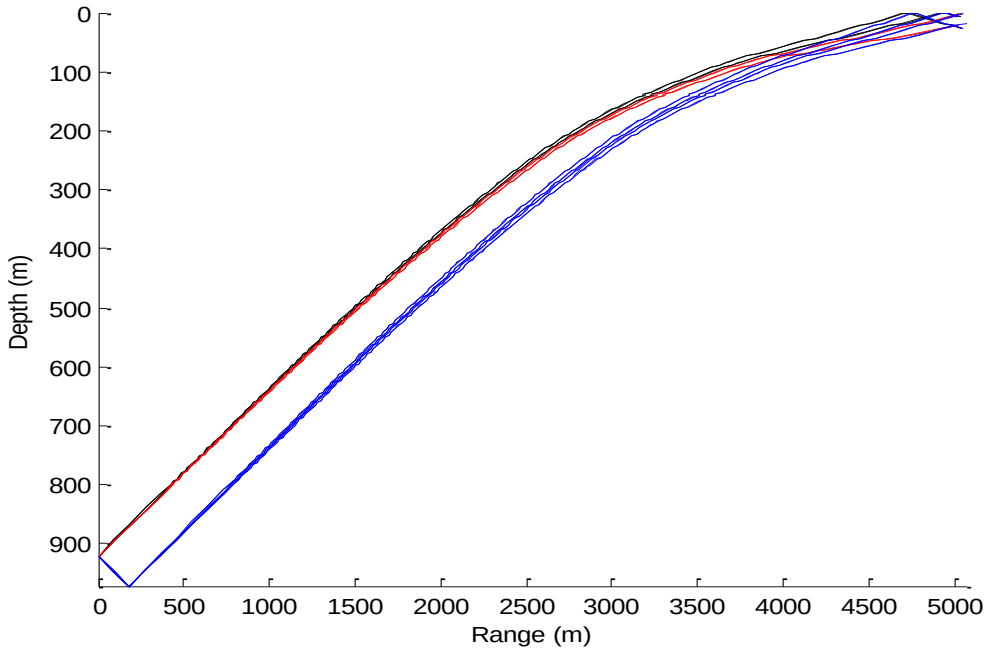

Figure 32. Illustration of eigenrays for a source at 920 m depth and receivers at 5 m and 23 m depths in Kauai environment.

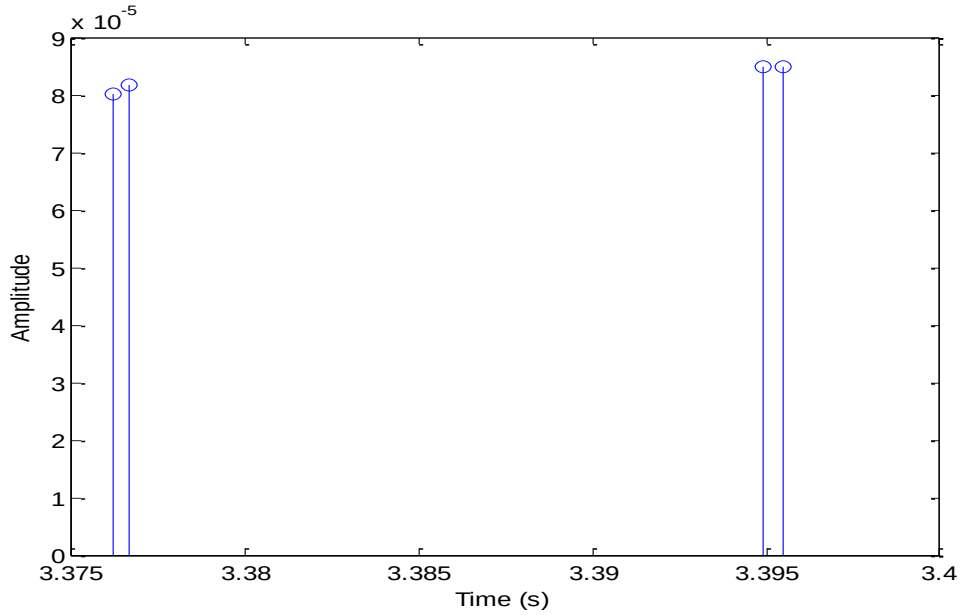

Figure 33. Arrivals with the receiver positioned at a depth of 5 m and the transmitter positioned at a depth of 920 m in Kauai environment.

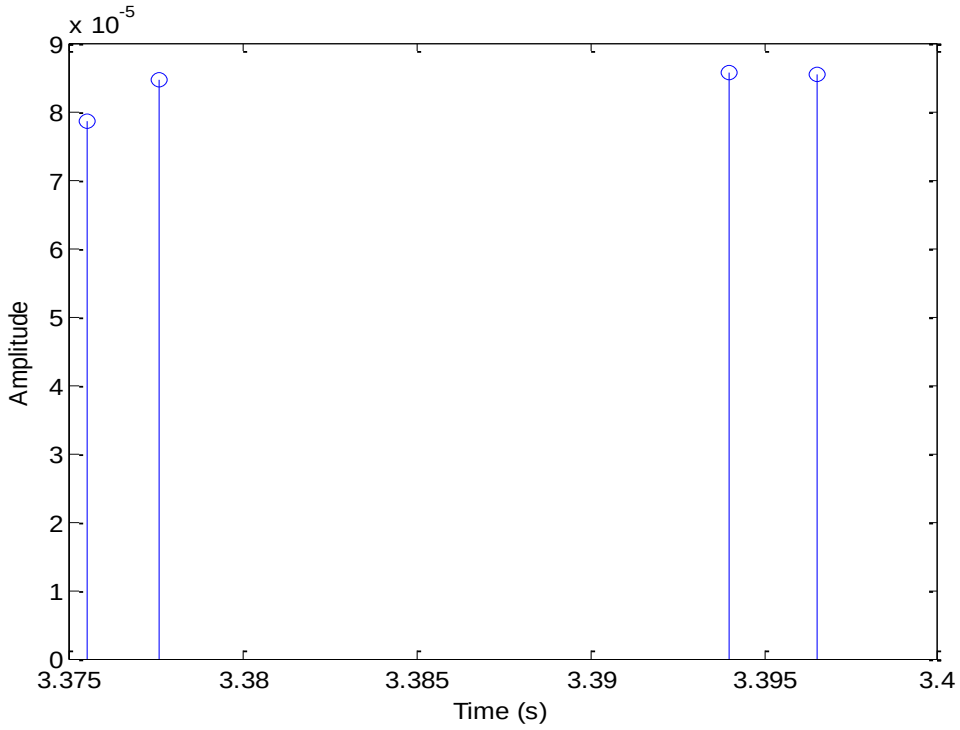

Figure 34. Arrivals with the receiver positioned at a depth of 23 m and the transmitter positioned at a depth of 920 m in Kauai environment.

For the receiver at 5 m depth, there are four arrivals in two different groups. The first group arrives at around 3.375 seconds, and the second group arrives at around 3.395 seconds. The rays arrive at the second receiver at 23 m depth almost at the same time interval as the first receiver, and there are two different groups and four arrivals as well. From the phase and the amplitude information, the arrivals were approximated and dB values of the arrivals were taken to represent the Rayleigh fading channel.

The sampling rate was chosen as $1/1000$ seconds, and the symbol rate was 500 symbols/second.

The quality in channel estimation is shown in the Kauai environment by taking the measurements up to 36 dB SNR. The normalized minimum-mean-square error plot for the estimated channels is illustrated in Figure 35.

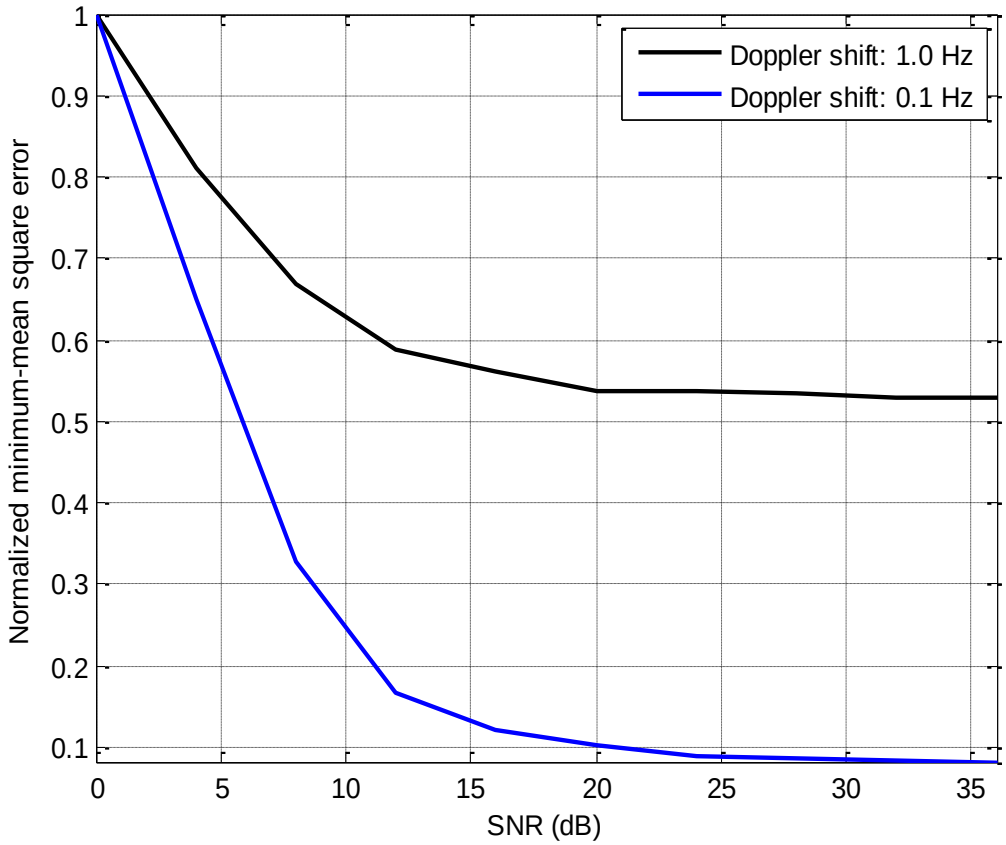

Figure 35. Normalized minimum-mean square error for channel estimation in Kauai environment where the transmitter is at 920 m, receivers are at the depths of 5 m and 23 m, and the horizontal range between the transmitter and receivers is 5 km.

When the Doppler shift frequency is 1.0 Hz, the error rate is much higher than the error found in shallow-water conditions, and the error rate is almost constant after around 20 dB SNR. On the other hand, when Doppler shift frequency is 0.1 Hz, the error is lower and continues to decrease for greater than 20 dB.

In Figure 36, the percent-error rate is shown for Kauai environment. According to this result, we see that the larger Doppler shift results in almost a constant value above some SNR. For a lower Doppler shift, the error is constant for larger SNR, and the channel estimation is better than for the larger Doppler shift.

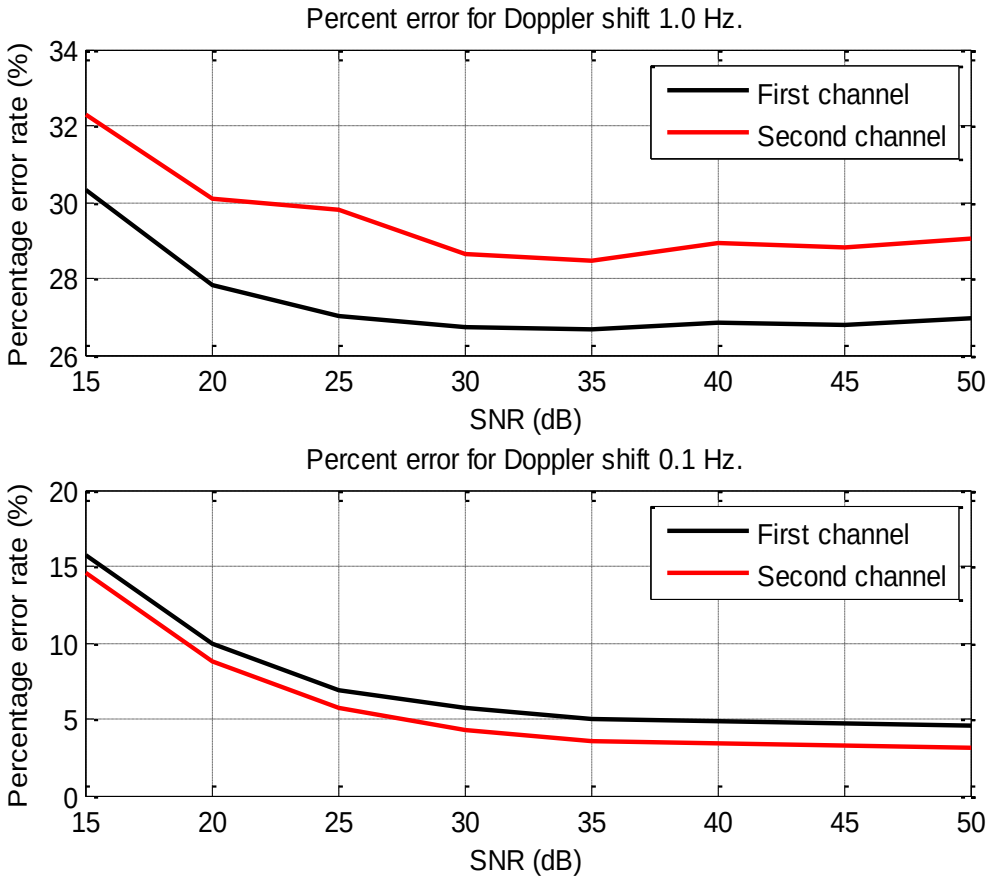

Figure 36. Percent-error rate of channel estimation in Kauai environment.

THIS PAGE INTENTIONALLY LEFT BLANK

VII. CONCLUSIONS

A. SUMMARY OF THE MODEL AND CONTRIBUTION

A two-receiver underwater acoustic communication system was presented in this thesis. Equalization and tracking of the acoustic channels characterized by considerable multipath were implemented with a Kalman filter algorithm. The acoustic channel was modeled with the Bellhop ray tracing model with its dependencies. A forward error-correction scheme and single carrier QPSK modulation was used. Since the channel is time-varying, the performance of the channel estimation was tested as a function of SNR and for different Doppler shift frequencies. Tracking of the time-varying channel by the proposed system is shown.

The Bellhop ray tracing model was used to model the acoustic channels, and emanating rays were shown according to the specified environment parameters. A Simulink model was used to simulate and show the results of the system for different parameters such as Doppler shift frequency and underwater acoustic environment variables. Two different channel types were implemented to show the validity of the model: a shallow-water acoustic channel and a deep-water Kauai environment. In both environments, the channels were estimated successfully with estimation success increasing as the Doppler shift frequency decreases. When the Doppler shift frequency was 0.1 Hz and the SNR large enough, the Kalman state filters calculated by the estimated channel coefficients recovered the transmitted sequence with zero error. The SNR needed to recover the transmitted sequence without error increases as the range between the transmitter and the receivers increases.

B. RECOMMENDATIONS FOR FURTHER WORK

With rapid advances in underwater acoustic communications, the proposed model can be improved to provide smaller error differences in channel estimation and to achieve better data rates. In this proposed model, the transfer function coefficients were calculated for each iteration, but this process increases computation time and reduces

efficiency. The calculations should be done for specific time intervals with an adaptive approach to obtain more efficiency from the system.

In this simulated system, the noise sources are assumed to be as AWGN, and for the future work, the model should be realized for non-Gaussian noise sources since the ambient noise in the ocean environments behaves in non-Gaussian manner. Instead of creating an artificial channel in a modeling program, the measurements should be taken in real environments to see how robust the system is.

Channel estimation quality was examined in this thesis, but BER was not calculated for specific SNR values. Although BER is inversely proportional to the channel estimation quality, it should be shown as a function of SNR for certain underwater environments.

APPENDIX A. MATLAB CODES

A. IMPULSE RESPONSE OF RAYLEIGH MULTIPATH FADING CHANNEL

The impulse response of the channel contains zero and non-zero values that are determined by the sampling rate of the source signal. The sampling rate determines the length of the channel impulse responses, and these channel impulse response coefficients are used in calculating the state-filter coefficients. Matlab codes related to finding these channel coefficients are shown below.

1. First Channel

```
function h1 = Channel(G1)

Fs = 2000;

D = [0 0.001 0.0025 0.004];

nd = round(D*Fs);

nd = nd+1;

h1 = complex(zeros(1,max(nd)));

G1 = [G1(1), G1(2), G1(3),G1(4)];

h1(nd) = G1;
```

2. Second Channel

```
function h2 = Channel(G2)

Fs = 2000;

D = [0 0.001 0.0025 0.004];

nd = round(D*Fs);

nd = nd+1;

h2 = complex(zeros(1,max(nd)));
```

```
G2 = [G2(1), G2(2), G2(3),G2(4)];

h2(nd) = G2;
```

B. TRANSFER FUNCTION OF KALMAN FILTER

The sum of two Kalman transfer function outputs give the estimate of the transmitted data sequence and this operation is repeated recursively with the estimated channel coefficients. Matlab code to calculate the transfer function coefficients is shown below.

```
%% Coefficients of transfer function

function [num1,num2,den] = Riccati(h1,h2)

coder.extrinsic('ss2tf');

coder.extrinsic('dlqe');

h1 = [h1 0]; % First channel

h2 = [0 h2]; % Second channel

N1=length(h1);

N2=length(h2);

N=max([N1,N2])-1;

% Defining state-space matrices

A=[-h1(2:N1)/h1(1);

  eye(N-1), zeros(N-1,1)];

B=[1/h1(1);

zeros(N-1,1)];

Bw=B;

C=h2(2:N2);

D = 0;
```

```
Q = 0.0001;

R = 0.0001;

G = Bw;

M = complex(zeros(length(A),1));

[M,P,Z,E]=dlqe(A,Bw,C,Q,R);

K=A*M;

Cx=[zeros(1,N-1),1];  % State  of x(n-N)

num1 = complex(zeros(length(A)+1,1));

num2 = complex(zeros(length(A)+1,1));

den1 = complex(zeros(length(A)+1,1));

[num1, den1]=ss2tf(A-K*C, B, Cx, 0,1);

[num2, den2]=ss2tf(A-K*C, K, Cx, 0,1);

den = den1;

end
```

C. IMPULSE RESPONSE MAGNITUDE DIFFERENCE

Estimation of the channel impulse response is tested with the actual channel response, and the Matlab code below calculates the error amount between the actual and the estimated channels.

```
%% Error calculation

for i = 1:length(h1)

h_tilde1(i,:) = h1(i,:)-h1_est(i,:);

h_tilde2(i,:) = h2(i,:)-h2_est(i,:);

error(i) = sqrt(sum(abs(h_tilde1(i,:)).^2) + sum(abs(h_tilde2(i,:)).^2));

end
```

```
error_f = mean(error);
%% Plotting the magnitude difference in magnitude
dB_val = [0:4:36];
error_DS1 = [0.8637,0.5250,0.2987,0.1988,0.1583...
            0.1443,0.1383,0.1366,0.1360,0.1359];
error_DS01 = [0.8559,0.4593,0.2342,0.1300,0.0789...
             0.0524,0.0362,0.0266,0.0213,0.0186];
plot (dB_val,error_DS1/max(error_DS1),'k');
hold on
plot (dB_val,error_DS01/max(error_DS01),'b');
axis tight
grid on
xlabel('SNR (dB)');
ylabel('Normalized minimum-mean square error');
title('Error difference magnitude for shallow acoustic channel');
legend('Doppler shift: 1.0 Hz','Doppler shift: 0.1 Hz');
hold off
%% Calculate in deep water
dB_val_deep = [0:4:36];
err_deep_1 = [1.2118,0.9822,0.8089,0.7120,0.6810...
            0.6516,0.6498,0.6464,0.6409,0.6401];
err_deep_01 = [1.1263,0.7315,0.3701,0.1803,0.1362...
             0.1145,0.1004,0.0967,0.0948,0.0924];
plot (dB_val_deep,err_deep_1/max(err_deep_1),'k');
```

```
hold on
plot (dB_val_deep,err_deep_01/max(err_deep_01),'b');
axis tight
grid on
xlabel('SNR (dB)');
ylabel('Normalized minimum-mean square error');
title('Error difference magnitude for Kauai deep acoustic channel');
legend('Doppler shift: 1.0 Hz','Doppler shift: 0.1 Hz');
hold off
```

THIS PAGE INTENTIONALLY LEFT BLANK

APPENDIX B. SIMULATION DIAGRAM

A. SIMULINK DIAGRAM OF PROPOSED MODEL

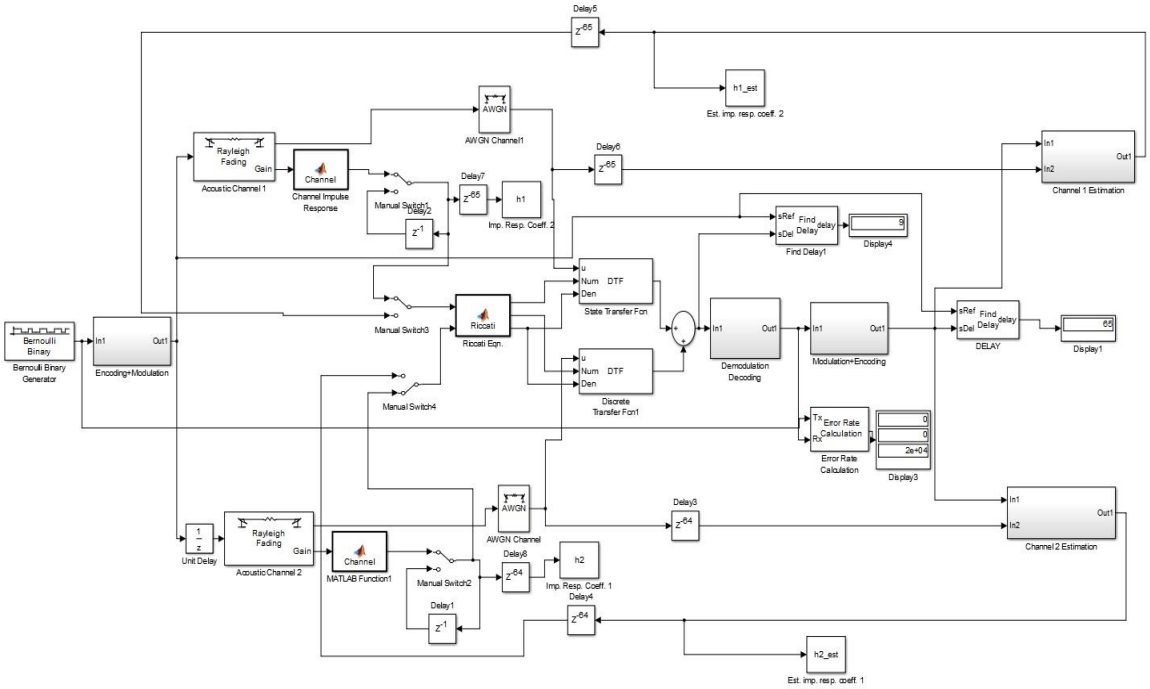

Figure 37. Simulink diagram of the proposed model.

THIS PAGE INTENTIONALLY LEFT BLANK

LIST OF REFERENCES

[1] S. Dessalermos, "Adaptive reception for underwater communications," Ph.D. Dissertation, Physics Dept., Naval Postgraduate School, Monterey, CA, 2011.

[2] M. Chitre, L. Freitag, E. Sozer, S. Shahabudeen, M. Stojanovic and J. Potter, "An architecture for underwater networks," *Asia Pacific OCEANS*, Singapore, 2007, pp. 1–5.

[3] L.M. Wolff, E. Szczepanski, and S. Badri-Hoeher, "Acoustic underwater channel and network simulator," *OCEANS*, Yeosu, Korea, 2012, pp. 1–6.

[4] A. Bouzoualegh, T. Val, E. Campo, and F. Peyrard, "Modeling and simulation of underwater acoustics communication based on stateflow and simulink models," *3rd Int. Conf.: Sciences of Electronic, Technologies of Information and Telecommunications*, Tunisia, 2005.

[5] UAN (2013). Underwater Acoustic Network website. [Online]. Available: http://www.siplab.fct.ualg.pt/UAN/

[6] R.H. Rahman, C.R. Benson and M.R. Frater, "Routing challenges and solutions for underwater networks," *Communications and Information Systems Conference (MilCIS)*, Canberra, ACT, 2012, pp. 1–7.

[7] W. Chen and F. Yanjun, "Physical layer design consideration for underwater acoustic sensor networks,"*3rd IEEE Int. Conf. on Computer Science and Information Technology (ICCSIT)*, Chengdu, China, 2010, pp. 606–609, vol. 9.

[8] P. Bouvet and A. Loussert, "Capacity analysis of underwater acoustic MIMO communications,"*OCEANS*, Sydney, NSW, 2010, pp. 1–8.

[9] Wines lab (2013). Wireless networks and embedded systems lab. [Online]. Available: http://www.eng.buffalo.edu/wnesl/underwater_sensor_networks.php.

[10] H.D. Trung and V.D. Nguyen, "An analysis of MIMO-OFDM for underwater communications,"*3rd Int. Congress on Ultra Modern Communications and Control Systems and Workshops (ICUMT)*, Budapest, Hungary, 2011, pp. 1–5.

[11] F. Qu, L. Yang and T.C. Yang, "High reliability direct-sequence spread spectrum for underwater acoustic communications," *Marine Technology for Our Future: Global and Local Challenges OCEANS*, MTS/IEEE Biloxi, Biloxi, MS, 2009, pp. 1–6.

[12] C. He, J. Huang, Q. Zhang, and X. Shen, "Single carrier frequency domain equalizer for underwater wireless communication," *WRI Int. Conf. on Communications and Mobile Computing*, Yunnan, 2009, pp. 186–190, vol. 1.

[13] S. Kim, J. Han, K. Kim, S. Baek, H. Kim, and C. Kim, "Experimental results of single carrier digital modulation for underwater sensor networks," *IEEE/IFIP International Conference on Embedded and Ubiquitous Computing*, Hong Kong, 2010, pp. 326–330.

[14] M. Tummala, "Ad-Hoc wireless networks," class notes for EC4745, Department of Electrical and Computer Engineering, Naval Postgraduate School, April 2014.

[15] CableFAX website. [Online]. Available: http://www.cablefax.com/tech/operations/testing/15131.html

[16] L. Zhong and N. Xiao-ling, "Comparison of equalization algorithms for underwater acoustic channels," *2nd Int. Conf. on Computer Science and Network Technology (ICCSNT)*, Changchun, China, 2012, pp. 2059–2063.

[17] S. Katwal, R. Nath and G. Murmu, "A simple Kalman channel equalizer using adaptive algorithms for time-variant channel," *Int. Conf. on Signal Processing, Communiation, Computing and Networking Technologies (ICSCCN)*, Thuckafay, 2011, pp. 178–181.

[18] F.B. Jensen, W.A. Kuperman, M.B. Porter and H. Schmidt, "*Computational Ocean Acoustics*," first edition, Springer-Verlag, New York, 2000.

[19] D. Kapolka, "Underwater acoustics," class notes for PH3452, Department of Physics, Naval Postgraduate School, February 2014.

[20] Miscellaneous Technical Articles by Dr. A.R. Collins Website. [Online]. Available: http://www.arc.id.au/UWAcoustics.html.

[21] R.P. Hodges, "*Underwater Acoustics Analysis, Design and Performance of Sonar*," John Wiley & Sons, 2010.

[22] A. Falahati, S.C. Batman and B. Woodeard, "A simulation model of fading in an underwater channel," *IEE Colloquium on Simulation Techniques Applied to Sonar*, London, England, 1988, pp. 6/1-6/4.

[23] M.A. Deaett and P.P. Audi, "Interleaver performance for FSK transmission on the acoustic fading channel," in *Proceedings of the Symposium on Autonomous Underwater Vehicle Technology*, Washington, DC, 1990, pp. 313–317.

[24] M. Stojanovic, "Underwater acoustic communications," in *Electro International Professional Program Proceedings*, Boston, MA, 1995, pp. 435–440.

[25] BELLHOP ray/beam model web site. [Online]. Available: http://oalib.hlsresearch.com/Rays/HLS-2010-1.pdf.

[26] J.C. Torres, "Modeling of high frequency propagation in shallow water," Master's Thesis, Physics Dept., Naval Postgraduate School, Monterey, California, 2007.

[27] A.B. Carlson, "*Communications Systems-An Introduction to Signal and Noise in Electrical Communication*," 3rd edition. New York: McGraw-Hill Book Company, 1986.

[28] D. Kong, "Simulation of coherent signals with forward error correction coding," Master's Thesis, Elec. and Comp. Eng. Dept., Naval Postgraduate School, Monterey, California, 2007.

[29] R. Cristi, "Wireless communications with Matlab and Simulink: IEEE802.16 (WiMax) physical layer," unpublished.

[30] M. Fargues, "Statistical digital signal processing," class notes for EC4440, Department of Electrical and Computer Engineering, Naval Postgraduate School, November 2013.

[31] D.G. Manolaikis, V.K. Ingle and S.M. Kogon, *Statistical and Adaptive Signal Processing.* Norwood, MA: Artech House, 2005.

THIS PAGE INTENTIONALLY LEFT BLANK

INITIAL DISTRIBUTION LIST

1. Defense Technical Information Center
   Ft. Belvoir, Virginia

2. Dudley Knox Library
   Naval Postgraduate School
   Monterey, California